

# Compact Nuclei in Galaxies at Moderate Redshift:II. Their Nature and Implications for the AGN Luminosity Function

Vicki L. Sarajedini

Steward Observatory, University of Arizona, Tucson, AZ 85721

Richard F. Green

NOAO<sup>1</sup>, P.O. Box 26732, Tucson, AZ 85726

Richard E. Griffiths and Kavan Ratnatunga

Carnegie Mellon University, Department of Physics, 5000 Forbes Ave., Pittsburgh, PA  
15213-3890

Received \_\_\_\_\_; accepted \_\_\_\_\_

---

<sup>1</sup>The National Optical Astronomy Observatories are operated by the Association of Universities for Research in Astronomy, Inc., under Cooperative Agreement with the National Science Foundation.

## ABSTRACT

This study explores the space density and properties of active galaxies to  $z \simeq 0.8$ . We have investigated the frequency and nature of unresolved nuclei in galaxies at moderate redshift as indicators of nuclear activity such as Active Galactic Nuclei (AGN) or starbursts. Candidates are selected by fitting imaged galaxies with multi-component models using maximum likelihood estimate techniques to determine the best model fit. We select those galaxies requiring an unresolved point-source component in the galaxy nucleus, in addition to a disk and/or bulge component, to adequately model the galaxy light.

We have searched 70 WFPC2 images primarily from the Medium Deep Survey for galaxies containing compact nuclei. In our survey of 1033 galaxies, the fraction containing an unresolved nuclear component  $\geq 5\%$  of the total galaxy light is  $9 \pm 1\%$  corrected for incompleteness. In this second of two papers in this series, we discuss the nature of the compact nuclei and their hosts.

We present the upper limit luminosity function (LF) for low-luminosity AGN (LLAGN) in two redshift bins to  $z=0.8$ . Mild number density evolution is detected of the form  $\phi \propto (1+z)^{1.9}$  for nuclei at  $-18 \lesssim M_B \lesssim -14$ . The LFs appear to flatten at  $M_B \geq -16$  and this flatness, combined with the increase in number density, is inconsistent with pure luminosity evolution. Based on the amount of density evolution observed for these objects, we find that almost all present-day spiral galaxies could have hosted a LLAGN at some point in their lives. We also comment on the likely contribution of these compact nuclei to the soft X-ray background.

*Subject headings:* galaxies:active-nuclei-starburst

## 1. Introduction

To better understand the nature of any class of extragalactic object, an accurate knowledge of the luminosity function (LF) over a wide range of absolute magnitudes and covering a range of redshifts is necessary. For active galactic nuclei (AGN) this has been attempted using quasars at the brighter, primarily high redshift end and Seyfert galaxy nuclei, considered to be their intrinsically fainter counterparts, at the low luminosity, low redshift end (Cheng et al. 1985; Huchra & Burg 1992). Understanding how the faint end of the AGN LF evolves is of particular importance for determining the frequency and total space density of these objects at earlier epochs. Models for quasar evolution can be much better constrained with accurate knowledge of the shape at the faint end. Koo (1986) explains how many of the models are difficult to discriminate when only luminous quasars are included since this end of the LF is a power-law with a slope that is almost identical at all redshifts.

Furthermore, AGN are likely contributors to the X-ray background and several studies have determined the contribution of luminous quasars to the diffuse background (e.g. Schmidt & Green 1986). How the low luminosity AGNs (LLAGNs) contribute to the diffuse X-ray background has been a question of interest for some time (Elvis et al. 1984; Koratkar et al. 1995). An accurate understanding of the behavior of the faint AGN LF and its evolution would help us to determine the global significance of their contribution to the soft X-ray background.

How then can LLAGNs be observed in higher redshift galaxies? The use of spectroscopic techniques becomes quite difficult at moderate redshifts. Even locally, the observation of broad emission lines, indicative of Seyfert 1 activity, or emission line flux ratios indicating Seyfert 2 or LINER activity requires that the nucleus dominate the galaxy light (e.g. Huchra & Burg 1992) or have adequate spatial resolution for subtraction of the galaxy

light from the nucleus (Ho et al. 1997a). At moderate redshifts LLAGNs become virtually impossible to observe from the ground becoming indistinguishable from central regions of enhanced star formation or finite central density cusps of spheroidal components.

The Medium Deep Survey (MDS) (Griffiths et al. 1994) is an HST key project yielding two to four parallel WFPC2 exposures per week, each containing  $\sim 300$  galaxies down to  $V \sim 23.5$  mag. This survey provides an ideal sample of distant field galaxies for which morphology and galaxy light profiles can be studied at sub-kiloparsec resolution. Typical galaxy redshifts extend to  $z \simeq 0.8$ . The set of Cycle 4, 5 and 6 images consists of  $\sim 150$  fields with both  $V(F606W)$  and  $I(F814W)$  exposures.

This database provides a unique opportunity to search for morphological evidence of AGN or other compact nuclear activity such as starbursts. The nuclear activity of Seyfert galaxies manifests itself morphologically as an unresolved point source in the nucleus of the galaxy. This is due to the fact that most of the emission is originating from a small region typically a few parsecs in diameter. For Seyfert 2 nuclei the emission is probably originating over the broader narrow-line region but is still highly concentrated at the nucleus having nuclear FWHM  $\lesssim 200$  pc (Nelson et al. 1996). This is in agreement with the recent WFPC2 study of Seyferts by Malkan et al. (1998). They were able to resolve the nuclei of almost all local Seyfert 2 galaxies whereas most local Seyfert 1 nuclei remained unresolved. The physical size of an unresolved region in a WFPC2 image at  $z \leq 0.8$  easily encompasses that for both types of Seyfert nuclei. Other enhancements of this size in a galaxy profile would include starburst regions and nuclear HII regions. Nuclear starbursts typically have sizes of a few hundred parsecs (e.g. Weedman et al. 1981 for NGC 7714) and nuclear HII regions may be even smaller. These stellar enhancements in a galaxy light profile would appear unresolved over the redshift range of interest ( $0.2 \lesssim z \lesssim 0.8$ ) unless  $H_o$  is very high. The typical late-type spiral bulge, however, has a diameter of  $\sim 1$  kpc (Boroson 1981) which is

resolved in the HST images.

Our study includes galaxies in 70 WFPC2 fields which have been modeled to search for unresolved nuclei likely to be AGN or compact regions of star formation, i.e. starbursts. The galaxy modeling is based on maximum likelihood estimates used to extract quantitative morphological and structural parameters of the faint galaxy images. All galaxies to  $I \lesssim 21.5$  in 64 MDS fields and 5 Groth survey strip fields (E. Groth, P.I., Prop ID 5090) as well as the Hubble Deep Field to  $I \lesssim 23.5$  (Williams et al. 1996) have been modeled in this way to reveal an unresolved nuclear component when present. Selection of AGN using this technique results in a magnitude-limited sample which is less biased towards galaxies dominated by the nucleus than are spectroscopically selected samples. In this way, we probe the intrinsically fainter population of AGN and starbursts out to intermediate redshifts for the first look at how this population of objects evolves.

In Sarajedini et al. (1998) (Hereafter referred to as Paper I), we discuss in detail the selection of fields and the procedure for fitting the galaxy light profiles. We also describe the criterion used for selecting those galaxies containing compact nuclei along with various simulations to determine the uniqueness of the galaxy model. In addition, we present in Paper I the ground-based spectroscopic data for about one third of our sample and describe the procedure of estimating redshifts for the remaining sample with  $\sigma_z \leq 0.1$  using V-I color, I magnitude, and the bulge-to-total luminosity ratio.

In this paper we focus on the analysis of the sample selected in Paper I. We discuss the properties of the host galaxies such as color, magnitude, size and Hubble type. These properties are then compared with those of local Seyferts and starburst galaxies. The colors of the nuclei are used to differentiate between Seyfert-like nuclei and young starburst nuclei based on colors from representative spectra of these objects. Using this information, we calculate the upper limit luminosity function for LLAGN in the magnitude range

$-20 \leq M_B \leq -14$  in two redshift bins out to  $z=0.8$  and compare it with the LFs of local Seyferts and moderate redshift QSOs. We also comment on the likely contribution of these nuclei to the soft X-ray background.

## 2. Properties of the Host Galaxies

The sample of 101 galaxies containing unresolved nuclei described in Paper I is large enough to study, with some statistical significance, the morphological and photometric characteristics of the nuclei and host galaxies. Here we examine the properties of the hosts and compare them with local AGN and starburst host galaxies. The colors of the nuclei themselves are discussed in section 3 and are used to answer questions concerning the nature of this population of objects.

### 2.1. Host Galaxy Types

When discussing the host galaxy types for the point source nuclei galaxies in our sample, it is very important to determine how well the bulge component is measured in these galaxies. This measurement effect was examined using Monte-Carlo simulations described in Paper I. The galaxies used in the simulation were originally fit with disk+bulge models before the simulated nuclear point source was added. Based on this *a priori* disk+bulge fitting, we have a known “input” bulge-to-bulge+disk ( $B/B+D$ ) luminosity ratio which can be compared with the measured  $B/B+D$  luminosity ratio when the simulated point source is detected in the galaxy.

These simulations show that for detections of point sources greater than 20% of the total galaxy light, the bulge is never detected regardless of the input bulge value. Our fitting technique is unable to separate and measure the bulge and point source components

when the point source is a large contributor ( $\geq 20\%$ ) of the total galaxy light. This is not the case for fainter point sources ( $\lesssim 20\%$ ) where the bulge is more accurately measured. We note that in all of the cases where the input bulge-to-total was zero, it was also measured as zero.

For point sources fainter than 20% of the galaxy light where the input bulge-to-total ratio is non-zero, we determine how often is it measured accurately and how often is it measured as zero. Figure 1a shows the fraction of galaxies where no bulge is detected for the simulated galaxies as a function of the actual input bulge-to-total luminosity ratio. The error bars represent the Poisson statistics based on the number of points in each bin. From this figure we see that as the bulge becomes more significant, it is more likely to be measured accurately and not go undetected.

We can apply this statistical result to the real sample of compact nuclei galaxies to determine what fraction of these galaxies may actually contain a significant bulge where none was measured in the fitted model. Of the 101 compact nuclei galaxies in our sample, only 8 have point source-to-total luminosity percentages greater than 20%. For these 8, no bulge is detected as we would expect based on the simulations. These galaxies, however, could contain a significant bulge component which is not being properly measured due to the bright point source nucleus. A hidden bulge component in these galaxies may be as much as 50% of the total light but is probably not dominating the host galaxy since spiral structure is seen upon examination of the galaxy images.

The remaining 93 galaxies have point source-to-total luminosity percentages less than 20%. Of these, 57 are measured to have no bulge component. We can estimate the fraction of the 57 that are statistically likely to contain a bulge based on Figure 1a. In this figure, the fraction of galaxies having measured bulge-to-bulge+disk luminosity ratios between 0 and 0.2 is high, indicating that a large fraction of host galaxies having bulge components

as large as 20% will be measured as having no bulge. Our 57 hosts with no detected bulge may contain bulges that are up to 20% of the total host galaxy light. Therefore, our first grouping of host galaxy types are those with  $0 \leq (B/B+D) < 0.2$  since it is difficult to differentiate these galaxy types with higher resolution. There are a total of 79 hosts in this grouping.

There are 9 galaxies measured with  $0.2 \leq (B/B+D) < 0.5$ . According to Figure 1a,  $59\% \pm 9\%$  of galaxies with this size bulge will be measured with no bulge when a point source (of less than 20% the galaxy light) is detected. If 9 galaxies have  $0.2 \leq (B/B+D) < 0.5$  then as many as 9 to 19 galaxies of this type will be measured with no bulge component. Three host galaxies fall in the  $0.5 \leq (B/B+D) < 0.8$  bin. Figure 1a indicates that  $21\% \pm 9\%$  of these galaxy types will be measured as having no bulge. Based on this percentage, we would expect one additional host galaxy with  $0.5 \leq (B/B+D) < 0.8$  to be measured as having no bulge component.

According to this analysis, the 57 host galaxies measured with no bulge component are likely to be comprised of 9 to 19 galaxies with  $0.2 \leq (B/B+D) < 0.5$  and 1 galaxy with  $0.5 \leq (B/B+D) < 0.8$ . Removing these 10 to 20 galaxies from the  $B/B+D=0$  bin allows us to statistically redistribute the host galaxy types based on our previous simulations. The solid line in Figure 1b is the measured  $B/B+D$  distribution for the 101 host galaxies containing compact nuclei. The dashed lines are the statistically redistributed histograms where the 2 lines represent the two extremes of the distribution. Here we have assumed that the 8 host galaxies with point source nuclei greater than 20% of the galaxy light have bulges less than 50% of the host galaxy light and could lie entirely in the  $0 \leq (B/B+D) < 0.2$  bin or the  $0.2 \leq (B/B+D) < 0.5$  bin.

The dashed lines in Figure 1b indicate that the actual number of host galaxies having  $0 \leq (B/B+D) < 0.2$  is likely to be from 58% to 76% of the 101 host galaxies in our sample.

Eighteen to 36% may have  $0.2 \leq (B/B+D) < 0.5$ . Only 6% are likely to have  $B/B+D \geq 0.5$ . We note, however, that the incompleteness estimates for detecting point sources in galaxies containing a substantial bulge is high. In Paper I we show that the completeness is typically 25 to 40% for galaxies with  $0.5 \leq (B/B+D) < 1.0$ . Therefore, there are likely to be 2.5 to 4 times as many point source nuclei present than were actually found in galaxies with large bulges.

Figure 1b shows that even at the extremes, the majority of host galaxies (58-76%) have small bulges indicating late-type spiral galaxy hosts. One-fifth to one-third may be early-type spirals with bulges greater than 20% of the galaxy light but less than 50%. We detect only 6% with bulges greater than 50% of the host galaxy light. Incompleteness corrections could increase this from 6% to  $\sim 10\%$  (see discussion in the following section).

To compare our sample with local host galaxy types of Seyferts and starbursts, we will assume a galaxy with  $B/B+D \leq 0.2$  is a late type spiral (Sc to Sb) and  $0.2 \leq (B/B+D) < 0.5$  is an early type spiral (Sa to S0). Although Hubble type does not depend on Bulge/Disk measurement alone we can estimate the approximate type based on a study of the luminosity distribution in nearby spiral galaxies (Boroson 1981). The CfA Seyfert galaxies studied in McLeod & Rieke (1995) had Hubble types ranging from S0 to Sc with no elliptical hosts. 45% were found in late type spirals and the remaining 55% in early type spirals. These Seyferts, although considered low-luminosity AGN, are likely to have intrinsically brighter nuclei than our sample since they were selected spectroscopically. However, a similar distribution is found in the Ho et al. (1997a) study of “dwarf” Seyfert nuclei in nearby galaxies. They find about 8% of the dwarf nuclei reside in ellipticals, while 46% are in S0 to Sa galaxies and another 46% reside in Sb through Sm galaxies. In contrast, Balzano (1983) finds that for starburst nuclei in local galaxies, 3% are in ellipticals, 30% are in early type spirals, and 67% are in late type spirals. Locally, starburst galaxies appear to favor

late type spirals more so than dwarf Seyfert nuclei and this causes the local starburst host type distribution to more closely resemble our host galaxy type distribution. However, our distribution would also be consistent with some combination of local Seyfert nuclei hosts and starburst nuclei hosts which is the expected mix of object types in our sample.

As part of this study, we also note the galaxies in our survey for which we obtained spectra and compare their Bulge/Total measurements with Hubble-types as estimated from their spectra. Kennicutt (1992) presents integrated spectra of nearby galaxies and compares emission and absorption features with Hubble class for normal and peculiar galaxies for a range of galaxy types. He finds that early-type galaxies from E's to Sa's have similar absorption feature spectra. H $\alpha$  + [NII] and [SII] become prominent for Sb's and later types. In Sc's through irregulars, we see many more emission lines such as [OIII], H $\beta$  and [OII].

In our spectra, 10 galaxies had wavelength coverage for H $\alpha$  detection. H $\alpha$  emission was observed in 9 of those galaxies all of which had Bulge/Total values less than 0.06, consistent with late-type spirals. The one without H $\alpha$  detected had Bulge/Total=0.3 which is consistent with an early-type spiral galaxy. For these cases, our Bulge/Total measurements appear to be consistent with spectroscopic classifications for these galaxies.

Out of the 29 spectra for which redshifts could be determined, 23 showed emission lines while 6 were only absorption spectra. Ninety-one percent of the emission line spectra galaxies had Bulge/Total $\leq$ 0.2 and 67% of the absorption spectra had Bulge/Total $\geq$ 0.2. Again, these statistics indicate that the majority of galaxies in our sample with measured spectra have spectral types consistent with their Bulge/Total measurements.

## 2.2. Comparison with Other Survey Galaxies

### 2.2.1. Morphology

It is interesting to compare the host galaxies of our compact nuclei with the entire sample of 1033 galaxies from the MDS, Groth strip, and HDF. As mentioned before, the measurement of Bulge/Total luminosity ratio gives us an estimate of the probable Hubble type for a galaxy. Figure 2 is the histogram of Bulge/Total values for the entire sample of galaxies in our survey. The hatched region is the true normalized histogram while the dotted line represents the fraction of galaxies found in each Bulge/Total bin defined in the previous subsection. This dotted line can be compared to the host galaxy Bulge/Bulge+Disk distributions in Figure 1b. All of the possible host galaxy distributions in Figure 1b are weighted towards later-type galaxies as compared to the total galaxy sample. In Figure 2, a larger fraction of host galaxies have  $0 \leq (B/B+D) < 0.5$  than survey galaxies. Although the largest fraction of survey galaxies also have  $0 \leq (B/B+D) < 0.5$ , there are many more with  $0.5 \leq (B/B+D) < 1.0$  than what is seen in the host galaxy sample.

This apparent discrepancy could be attributed in part to incompleteness in detecting nuclei in galaxies with large bulges. We can correct for this effect using conservative completeness estimates calculated in Paper I (90% completeness for  $(B/B+D)=0$ , 55% completeness for  $0 < (B/B+D) \leq 0.4$ , 43% for  $0.4 < (B/B+D) \leq 0.8$ , and 38% for  $(B/B+D) > 0.8$ ). Adjusting our numbers in each  $B/B+D$  bin accordingly indicates an increase in the number of host galaxies with  $0.5 \leq (B/B+D) < 1.0$  from 6% to  $\sim 10\% \pm 2.5\%$ . This fraction is still significantly lower than the  $\sim 15\%$  of all survey galaxies of this type. Based on this distribution, the host galaxies containing compact nuclei do appear to favor galaxies with bulges contributing less than 50% of the total galaxy light.

### 2.2.2. Size and Magnitude

We investigate how the compact nuclei galaxies vary in angular size and apparent magnitude from the entire sample of survey galaxies in Figure 3. Figure 3a shows the angular size (natural log of the half-light radius) in arcsec vs. the apparent I band magnitude of the survey galaxies (open circles) and the host galaxies (filled circles). The typical limiting magnitude for MDS and Groth strip fields at  $I \simeq 21.5$  is apparent in the diagram. Most of the fainter galaxies are from the Hubble Deep Field. The smallest host galaxies are also from the HDF and are as small as 2 pixels ( $0.2''$ ) in radius. It appears that few of the large but faint galaxies, possibly low surface brightness galaxies, appear to host point source nuclei. This trend is further revealed in Figure 3b which is the normalized distribution of the half-light radii for the host galaxies (hatched region) and the non-host galaxies (solid line). The host galaxy distribution peaks at a smaller half light radius ( $hlr \simeq 0.45''$ ) than the non-host galaxies ( $hlr \simeq 0.72''$ ) and also cuts off at a half-light radius of  $\sim 1.9''$ . A KS test conducted on both the size and magnitude distributions of the two populations indicates that they are drawn from different parent populations at the 80% significance level. A possible explanation is that these galaxies may not contain enough mass to sustain a starburst nucleus or AGN. Recent work by Schombert (1998) has shown that HI-rich, low surface brightness galaxies have a greater chance of hosting LLAGN than other magnitude limited, late-type galaxies. This seems to indicate that the gas mass is an important factor in the existence of an active nucleus. Additionally, some mechanism is usually required to transport fuel to the nucleus. Mihos et al. (1997) shows through numerical simulations that low surface brightness galaxies are stable against the growth of bar instabilities, inhibiting a strong inflow of gas to the galaxy center for fueling a nuclear starburst or AGN. Although our nuclei are intrinsically faint, this observation implies that some limiting mass or ability to transport matter to the nucleus is necessary for their formation and duration.

### 2.2.3. Axis Ratios

Optically selected AGN have been observed to avoid edge-on spirals (Keel 1980; McKleod & Rieke 1995). Figure 4 shows the distribution of axis ratios for the disks of our host galaxies. We have included only those hosts that are disk-dominated, containing bulges less than 20% of the total galaxy light. The distribution is normalized by dividing the axis ratio distribution of host galaxies by the same distribution for the total sample of survey galaxies which are also disk-dominated. This normalizes the axis ratio distribution so that each bin represents the fraction of all disk-dominated galaxies with the specified axis ratio which contain compact nuclei. There is an observed drop in the fraction of hosts with disk axis ratios ( $b/a$ )  $\lesssim 0.4$ . However, this drop is much less significant than that observed in the spectroscopically selected CfA Seyferts. Lawrence and Elvis (1982) found that an inclination bias does not appear in hard X-ray selected samples of AGN. They conclude that selection biases seen in other samples are due to obscuration in a flattened disk parallel to the plane of the host galaxy. Although the axis ratio distribution of our data reveals a slight bias against edge-on host galaxies, our morphological selection technique appears to be less affected by this type of obscuration.

### 2.2.4. Galaxy Color

Finally, we examine how the colors of the host galaxies compare with the non-host galaxies. First we must understand the accuracy of the host colors. Our Monte Carlo simulations in Paper I show that the bulge component of a host galaxy is often undetected when a nuclear point source is fit. At the same time, these simulations show that the point source magnitudes are well determined within the errors. Therefore, the undetected bulge component does not appear to be mistakenly measured as part of the point source. How then does the missing bulge component effect the magnitude and consequently the

color measurement for the host galaxy? We again look at the Monte-Carlo simulations from Paper I to compare the *input* galaxy colors to those measured for the galaxy when a simulated point source is detected in the nucleus. For 389 galaxies in the simulation where the point source nucleus was detected (in both or only one filter) the distribution of color errors was centered around zero with  $\sigma_{(V-I)}=0.37$ . This indicates that we are not seeing a systematic offset between the measured and true color of the host galaxy which might be expected if the bulge were being completely ignored in the model fitting. Instead, when the bulge is not detected, it seems to be absorbed in the disk component such that the host galaxy color is not systematically affected. Keeping in mind the typical errors in determining the host galaxy color, we compare them to those of galaxies in our survey without unresolved nuclear components.

Figure 5a is the color-magnitude diagram for the galaxies in our survey where the open circles are non-host galaxies and the filled circles are the host galaxies. We have removed the color contribution of the nucleus from the integrated galaxy color to produce the host galaxy V-I color. In order to directly compare the sample of host galaxies with a similar representation of the survey galaxies, a random subset of the 1033 survey galaxies was selected based on the host galaxy distribution in Figure 1b (short-dashed line). This allows us to compare our host galaxy colors to those of survey galaxies morphologically similar to our hosts. Figure 5b shows the normalized histogram of the V-I colors for the compact nuclei host galaxies (hatched region) where the subset of similar survey galaxies is represented by the solid line. A KS test for these color distributions yields a probability of 0.43, where low KS probabilities indicate that two populations are not drawn from the same parent distribution. This result indicates that the two distributions are not statistically different. The mean color for the host galaxies is  $\mu_{(V-I)}=0.97$  while the mean survey galaxy color is  $\mu_{(V-I)}=1.03$ . In general, we find that the host galaxy colors are like those of other morphologically similar galaxies in the field with a slight tendency to be bluer.

### 2.3. Host Galaxy Absolute Magnitudes

Using the spectroscopic and photometric redshifts for each galaxy containing an unresolved point source nucleus, we can examine the absolute magnitudes of the host galaxies as they compare with other galaxies. Figure 6a is the histogram of absolute rest-frame B magnitudes for the 101 host galaxies which contain unresolved nuclei using  $H_o=75$  km/s/Mpc and  $q_o=0$ . The B-band luminosities for the galaxies were derived from their V magnitude, V-I color and redshift. This information is used to select a non-evolving model spectral energy distribution from the set described in Gronwall and Koo (1995). The models are based on those of Bruzual and Charlot (1993). The k-corrections are small (typically  $\lesssim 0.3$  mag) since the V magnitude is roughly rest-frame B at the median redshift of our survey ( $z \simeq 0.35$ ).

Our luminosity distribution peaks at  $M_B \simeq -20.4$  which is approximately  $L^*$ . For comparison with the following samples, this corresponds to a peak at  $M_B \simeq -21.3$  with  $H_o=50$  km/s/Mpc. The luminosity distribution of normal spiral galaxies peaks at  $M_B = -20.6$  ( $H_o=50$  km/s/Mpc) (Christensen 1975), somewhat fainter than our sample of compact nuclei galaxies. Interestingly, Yee (1983) found the peak luminosity of Seyfert hosts from the Markarian survey to be  $M_B = -21.3 \pm 0.8$  which is strikingly similar to our sample. From this observation he argues that the Seyfert phenomenon tends to occur more often in the luminous end of the spiral population. According to the present study, this trend may also hold true for galaxies hosting compact nuclei. This brighter absolute magnitude for AGN hosts is also seen, though to a lesser degree, for X-ray selected AGN where the peak luminosity is  $M_B = -20.9$  (Kotilainen & Ward 1994).

We can compare our distribution to the dwarf seyfert nuclei hosts of Ho et al. (1997a) (Figure 6b) and the distribution of galaxies containing HII nuclei from Ho et al. (1997b) (Figure 6c) which were derived using  $H_o=75$  km/s/Mpc. These samples provide an

interesting comparison since the *nuclear* luminosities are closer to those of our sample than other spectroscopically selected AGN. The luminosity distributions are similar among the three samples. Although the peak luminosities are close, our sample does appear to drop off faster on the low luminosity side of the distribution. This is most likely caused by the nature of our magnitude-limited survey as it is observed over a range in redshift. As we observe at higher redshifts, intrinsically fainter galaxies are missed. Accounting for this discrepancy, we observe no evidence for evolution in the luminosity of AGN or starburst host galaxies out to  $z \simeq 0.8$ .

### 3. The Colors of the Point Source Nuclei: Clues to Their Nature

Model fitting of the point source component allows us to separate the color of the nucleus from that of the host galaxy. Of the 101 nuclear point sources detected, 93 were detected in the I filter image, 80 were detected in the V filter image, and 72 were detected in both filters allowing for a V-I color to be determined. This result leaves 29 point sources with no color information. There are a few reasons for not detecting the point source in one of the filters such as 1) the point source is too faint in one filter, 2) the point source does not converge properly in one filter making its magnitude unreliable, and 3) the image is too noisy in one filter for a point source to be detected. Of these 29, 5 were not detected in the other filter because of non-convergence of the model, 7 were not detected because of additional noise elements in that filter, and 17 were not detected because the point source was too faint in that filter. For these 17, we can determine a limit for the point source color assuming the point source in the other filter is fainter than 1% of the total galaxy light. For the other 12 point sources detected only in one filter, we cannot constrain the nuclear color.

Figure 7a shows the V-I colors of the point source nuclei vs. their host galaxy V-I colors. Here we have plotted the 72 points having color information with their appropriate

error bars. The 17 points with a point source color limit, due to non-detection in one filter, are marked with an arrow. Within the errors of the point source colors, the majority of point source nuclei are the same color as the underlying host galaxy. The large errorbars on the point source colors cause the correlation coefficient between the point source and host galaxy colors to be small indicating a low probability of correlation. In Figure 7b we show the generalized histogram of color differences between the host and point source where point sources bluer than the host are positive and those redder than the host are negative. This histogram is made by allowing each point to be represented as a gaussian with the calculated  $1\sigma$  error defining the width of the gaussian. The histogram is the summation of these gaussians. It does not include the 17 points with only color limits. The peak of this distribution occurs at  $\mu=-0.05$ , essentially zero, and the FWHM of the distribution is 1.52. The nuclear colors are in general the same as the host galaxy colors with a large spread in the distribution. Nuclei which appear bluer than the host can be explained as either young starburst nuclei or unobscured AGN. However, a nucleus can appear redder than the host if there is sufficient dust present or excess star formation in the disk causes the underlying galaxy to appear bluer.

It is also interesting to see how the nuclear colors compare with the color of the bulge where it is detected in both the V and I filters. Again, we first must understand the errors in the bulge colors as determined from the Monte-Carlo simulations. Based on comparison of the input bulge colors of the simulation galaxies to the measured bulge colors when a point source nucleus is detected, we determine the error in bulge color to be  $\sigma_{V-I}=0.85$ . This error is large but not unexpected since the bulge component appears to be the most difficult to measure accurately when a point source nucleus is detected in the galaxy. Again, there is no systematic color difference in the bulges observed in the simulation galaxies when a point source is detected. We apply the determined color error for bulges to our data to investigate any trends in the relationship between the nuclear and bulge colors.

Figure 8a is the point source color vs. the bulge color for the 17 galaxies where both a point source and bulge color were measurable. We have applied the determined bulge color error and point source color errors. Because these errorbars are so large, this figure is not useful for studying individual cases. In Figure 8b we show the generalized histogram of the color difference between the point source and bulge components. The histogram is made in the way described for Figure 7b. This figure allows us to observe any trends in the color difference while taking into account the errors in the individual points. The mean color difference between the bulge and the point source nucleus is  $(V-I)_{bulge} - (V-I)_{nucleus} \simeq 0.5$ . This indicates that in general, the nuclear colors are bluer than the bulge. This is expected if the bulge represents an older population than the nucleus or if the nucleus has typical non-thermal source colors.

Studying the nuclear colors allows us to look more deeply into the question of their nature. In the case of detection in a bulge dominated system, the color of the nucleus plays a role. As discussed above, we require the nucleus to be a different color from that of the underlying bulge to ensure that it is not merely an unresolved region of the bulge. Are there objects, besides Seyferts and starbursts, that could appear unresolved in an elliptical or bulge dominated galaxy and would be composed of a different stellar population from that of the bulge so that it would appear a different color? One additional possibility is a merger remnant. Theoretical and observational evidence suggests that major mergers, where the galaxies are of almost equal mass, form elliptical remnants (Hibbard et al. 1994 and references therein). In the case of the merger remnant NGC 3921, an unresolved nucleus is observed in an  $r^{1/4}$  profile galaxy (Schweizer 1996). The color gradient of the remnant indicates a redder nucleus than the remaining galaxy body. Such remnant nuclei could exist in our sample, although the small number (6%) of elliptical hosts suggests they would be a minor contributor to the population. There is also the possibility that minor merger remnants in the centers of galaxies could reveal themselves as unresolved nuclei of a

different stellar population than the host galaxy. It is unclear at this time how often such an object might occur in our survey.

With the spectroscopic and photometric redshifts of each host determined, we can examine any trends in the nuclear colors with redshift. This information is important in determining the true nature of the nuclei. Figure 9 shows the V-I colors of the nuclei plotted against their determined redshift. Errorbars in the redshift direction clearly differentiate between those objects with photometric redshifts ( $\sigma_z \simeq 0.9$ ) and those with spectroscopic redshifts. Open circles are those point sources with only limiting color information. To interpret this figure, we must understand how the colors of starbursts, AGN or any other stellar population thought to be present in our nuclear sample behave as a function of redshift. This modeling is explored in the following section.

#### 4. Synthetic V-I colors for AGN and Star Clusters: Comparison with the Nuclear Colors

The V-I colors of the point source nuclei in our sample provide important information to help us to understand their nature. To determine if the nuclei are starbursts or AGN, we must first understand the colors of these different objects. Most starburst and AGN photometry (other than that of bright QSO's) has been done at low redshifts. To simulate the effects of K-corrections on the object colors and therefore provide a more realistic comparison with our data, we use representative spectra to calculate synthetic V-I colors for AGN and starbursts with the HST F606W (V) and F814W (I) filters.

To simulate colors for the AGN nuclei, we use spectra from Kalinkov et al. (1993) for Seyfert 1, 1.5 and 2 galaxies where the nuclear activity dominates the spectrum. These spectra, which were produced by averaging the spectra of several reliably classified AGN

in each class, are shown in Figures 10a, 10b and 10c. Spectra of star clusters of various ages are used to simulate the appearance of certain isochronic stellar populations present in the nuclei sample. The spectra are from E. Bica and are available as part of a database of spectra for galaxy evolution models (Leitherer et al. 1996). Figure 10d is an integrated spectrum of HII regions, representing a very young population or current starbursting nucleus. Figure 10e represents a star cluster with age  $\simeq 10$  Myr and  $[Z/Z_{\odot}] \simeq -0.25$ . Figure 10f represents a star cluster with age  $\simeq 25$  Myr and  $[Z/Z_{\odot}] \simeq -0.4$ . The ages of the star cluster spectra shown in Figures 10g through 10i are 80 Myr, 200-500 Myr and 1-2 Gyr, respectively. Their respective metallicities are -0.5, -0.6 and -0.5.

To simulate the effects of redshift in our sample, the spectra were stepped incrementally in redshift to  $z \sim 0.8$  and the IRAF task CALCPHOT was used to determine the V-I colors of each object at a range of redshifts. CALCPHOT utilizes the appropriate HST filter response which is convolved with the spectra to produce accurate synthetic colors. Figure 11a shows the V-I colors for the 3 types of Seyfert galaxies as a function of redshift. The solid line is the Seyfert 2 color, the short dashed line is the Seyfert 1.5 and the long dashed line is the Seyfert 1. The majority of nuclei are consistent with the Seyfert colors within the errorbars. The two spectroscopically identified Seyfert 1s in our sample at  $z=0.45$ ,  $V-I=0.89$  and  $z=0.99$ ,  $V-I=0.22$  are consistent with the Seyfert 1 colors. Of the 89 point source nuclei with measurable colors or color limits, 8 are bluer than the Seyfert colors by more than  $1\sigma$  while 8 are redder. The latter sample, however, could be explained with moderate amounts of reddening due to dust.

Figure 11b shows the V-I colors for the various star cluster spectra shown in Figures 10d through 10i as a function of redshift. The solid line is the integrated HII region color. This locus represents the color a young starburst would have in our sample. The color varies with redshift as different emission lines in the spectrum pass through the V and I filters.

The blueward shift in the HII region color at  $z \simeq 0.35$  is caused by the  $4959\text{\AA}$  and  $5007\text{\AA}$  [OIII] and  $\text{H}\beta$  emission lines moving into the V filter. The remaining lines are specified in the figure caption and represent the other star clusters with increasing age corresponding to redder colors. The majority of the point source nuclei are consistent with the colors of intermediate aged star clusters. Five of the 8 galaxies which were too blue to be consistent with Seyferts fall within  $1\sigma$  of the HII region color at  $z \lesssim 0.4$ . Another one of these 8 point sources at  $z=0.60$ ,  $\text{V}-\text{I}=-0.10$  has a color consistent with that of a 25 Myr old cluster. Together, these 6 point sources have colors more consistent with those of star clusters than Seyfert nuclei. The other 2 point sources too blue to be Seyferts are also inconsistent with the star cluster colors.

The synthetic colors show that the vast majority of the nuclei in our sample have colors consistent with Seyfert-like nuclei *and* intermediate aged star clusters. A small number (6 out of 89) have colors too blue to be Seyferts but are consistent with young or intermediate aged star cluster colors. These 6 are likely to be starburst nuclei. The main population, however, cannot be identified explicitly as either Seyfert-like or starburst-like based on the  $\text{V}-\text{I}$  color alone. We assume that the remaining sample of 95 point sources, which includes the 12 point sources with no measurable color, consists of some combination of starbursts and Seyfert nuclei. The remaining 95 point sources represent an upper limit sample of AGN-like nuclei. In the next section, this sample is used to determine an upper limit on the AGN luminosity function at low luminosities.

## 5. The Number Density and Luminosity Function for Unresolved Nuclei

The luminosity function of AGN as a function of redshift provides much needed information about how this population of objects changes with time. Understanding the population as a whole may allow us to understand better the physics of QSOs. In addition,

accurate knowledge of the AGN LF is important for understanding their contribution to the soft X-ray background.

The bright end of the QSO LF has been well studied as a function of redshift (e.g. Hartwick & Schade 1990, and references therein). To study the faint end, Seyfert galaxies have been observed locally through spectroscopic surveys (Cheng et al. 1985; Huchra & Burg 1992). However, these surveys tend to include only bright Seyfert nuclei that dominate the galaxy light. Fainter nuclei would not be spectroscopically selected since the host galaxy light would dilute the nuclear emission. Morphologically, such faint nuclei can be detected if the nuclear light can be disentangled from the host galaxy. In this study we have separated the nuclear and galaxy light using 2-dimensional maximum likelihood galaxy modeling. This method allows us to study unresolved nuclear sources in galaxies out to moderate redshifts to fainter limiting magnitudes than previously observed.

Before constructing the luminosity function, we first compare the fraction of galaxies containing compact nuclei with the fraction of Seyfert galaxies determined locally and at moderate redshifts. As mentioned previously, Huchra & Burg (1992) (hereafter HB) have studied local Seyferts from the CfA redshift survey and find the percentage of galaxies containing Seyfert 1 and 2 nuclei to be  $\sim 2\%$ . Their study included Seyfert nuclei extending to  $M_B \lesssim -17$ . Maiolino & Rieke (1995) examined a sample of Seyfert galaxies closer than the CfA sample and were able to detect fainter nuclei since the nuclear spectra were less diluted by the host galaxy light. They found the percentage of Seyferts to be 5% and possibly as high as 16%. The majority of the additional objects in this study were Seyfert 2s which are underluminous in the optical with respect to type 1 Seyfert nuclei. Active nuclei were detected in this study to  $M_B \lesssim -16$ . In Paper I, we find the fraction of all galaxies in our survey containing compact nuclei to be  $16 \pm 3\%$  including nuclei  $\geq 3\%$  of the galaxy light corrected for incompleteness. This fraction is very similar to that found by Maiolino &

Rieke for local Seyferts, although our sample includes nuclei at least a magnitude fainter.

Ho et al. (1997a) find the percentage of local galaxies containing faint Seyfert nuclei to be 11% with LINERs (low-ionization nuclear emission line regions) occupying an additional 19% of galaxies. They find the fraction of galaxies containing HII nuclei to be 42% of all galaxies. These nuclei are extremely faint based on their emission line luminosities ( $L(H\alpha) \leq 10^{40}$  ergs s $^{-1}$ ). Many of these nuclei are too faint for morphological detection as a point source in the host galaxy and were identified based on emission lines alone. These results are intriguing as they suggest that the possible fraction of local galaxies containing low-luminosity active nuclei may be as high as 30% (including LINERS). Since optical integrated magnitudes for these AGN and HII nuclei have not been determined, we cannot directly compare the fraction of galaxies in the present study containing compact nuclei with the fraction of galaxies containing faint AGN and HII nuclei from Ho et al.

At moderate redshifts ( $z \leq 0.3$ ), Tresse et al. (1996) have searched for evidence of nuclear activity in the Canada-France Redshift Survey (CFRS) and find that 17% of all galaxies have emission line flux ratios consistent with active nuclei galaxies. Since these objects are spectroscopically selected, this survey contains only those nuclei which dominate the host galaxy light such that their emission lines are not greatly diluted by the underlying galaxy. When they correct for possible stellar absorption of the Balmer lines due to the host galaxy, the fraction of galaxies displaying activity is 8%. Their results are somewhat inconsistent with those of Maiolino & Rieke since the fraction of higher redshift galaxies containing active nuclei identified by Tresse et al. appears to be less than that for local Seyfert nuclei. Such inconsistencies highlight the need for space density studies of LLAGN at moderate redshift.

## 6. The Upper Limit Luminosity Function for LLAGN

In section 4 we selected a subsample of our compact nuclei which have colors consistent with those of Seyfert nucleus-dominated galaxies based on synthetic photometry of representative spectra. However, the colors are also consistent with intermediate aged starburst nuclei making this subsample an upper limit estimate on the number density of AGN in this survey. This subsample can be used to construct the upper limit luminosity function for faint AGN out to redshifts of  $z \simeq 0.8$ , providing the first look at the shape and parameters of the AGN LF in this luminosity and redshift regime.

### 6.1. LF Calculation

To calculate the luminosity function for our sample of 95 compact nuclei with colors consistent with AGN-like nuclei, we use the  $1/V_A$  technique described fully in Schmidt and Green (1983) where  $V_A$  is the accessible volume in which each object can be observed. This technique allows us to calculate the space density of the compact nuclei as a function of their absolute magnitudes and redshifts. This quantity is symbolically defined as  $\phi(M, z)$ . To calculate absolute magnitudes from the nuclear apparent magnitudes we use the equation

$$M_B = B - 5 \log A(z) + 2.5(1 + \alpha) \log(1 + z) - 5 \log(c/H_o \times 10^6) + 5 \quad (1)$$

where  $B$  is the apparent magnitude,  $c$  is the speed of light in km/s,  $H_o$  is the Hubble constant in  $\text{km s}^{-1} \text{Mpc}^{-1}$ , and  $\alpha$  is the spectral index defined by

$$F_\nu \propto \nu^\alpha \quad (2)$$

The quantity  $A(z)$  is the bolometric luminosity distance defined as

$$A(z) = z \left\{ \frac{1 + z(1 - q_o)}{[(1 + 2q_o z)^{1/2} + 1 + q_o z]} \right\} \quad (3)$$

The term  $2.5(1+\alpha)\log(1+z)$  in equation 1 represents the effect of the redshift on measurements through a fixed color band (i.e. the K-correction). Since we do not have apparent B magnitudes, we determine them from the apparent V magnitude and the spectral energy index,  $\alpha$ , according to the following equation

$$B - V = \alpha 2.5 \log_{10}(\lambda_B/\lambda_V) \quad (4)$$

where  $\lambda_B=4500\text{\AA}$  and  $\lambda_V=6060\text{\AA}$  for the HST filters. We assume the width of the filter bands to be comparable. With  $\alpha=-1.0$ , this equation yields  $B-V=0.32$ . We use  $\alpha=-1.0$  or  $-0.5$  in later calculations for direct comparison with other LFs in the literature. Based on the spectra for Seyfert-nucleus dominated galaxies described in section 4, their rest frame B-V colors are 0.34, 0.50 and 0.71 for Seyfert 1, 1.5 and 2 galaxies respectively. Our choice of  $\alpha$  for the sake of comparison may be somewhat blue for the typical object in our survey, however, the choice of magnitude bin sizes is much larger than this error in the magnitude.

The absolute magnitude of each point source in the sample is determined according to the above equations. With the absolute magnitude we determine the maximum redshift at which the point source would be observable in each of our 70 WFPC2 fields. The limiting point source magnitude per field is determined for each object by calculating its apparent magnitude had it been detected in a galaxy at the limiting galaxy magnitude of each field in the study. This point source limiting apparent magnitude per field is based on the observed percentage of galaxy light contained within the nucleus. The maximum redshift per field is then used, in combination with the total area of the field in steradians, to determine the comoving volume over which each object is observable in each survey field. The summation of the volumes for each field is the accessible volume for that particular object. The quantity  $\phi$  is then determined as a function of absolute magnitude and redshift through the following summation

$$\phi(M, z)dM = \sum_{j=1}^n \frac{1}{V_a^j} \quad (5)$$

for  $z_j \in (z_1, z_2)$  and  $M_j \in (M_1, M_2)$  where  $M_1 = M - dM/2$ ,  $M_2 = M + dM/2$ ,  $z_1 = z - dz/2$ , and  $z_2 = z + dz/2$ . The integer  $j$  denotes individual galaxies in each absolute magnitude and redshift bin. In this way, the number density is determined for a discrete luminosity interval and a discrete redshift interval.

Because of the large errorbars in redshift for the photometrically determined objects in our sample, an additional consideration is made in determining the luminosity function. Each individual object is considered as a Gaussian distribution in redshift space. In this way, each object is spread over its appropriate luminosity range in the LF calculation. The determination of  $\phi$  is then computed by

$$\phi(M, z)dM = \sum_{k=1}^n \frac{(\text{Weight})}{V_a^k} \quad (6)$$

so that only the appropriately weighted portion of each point is considered in the number density calculation in each specific luminosity and redshift interval. The value of  $k$  represents the individual fractions of each galaxy so that  $n$  is the number of galaxies multiplied by the number of divisions in redshift space over which each object is distributed.

We also correct for incompleteness in our LF based on our analysis from Paper I. For each point source in the survey, the level of incompleteness is determined depending on the point source-to-total luminosity ratio of the object. This factor is then multiplied with  $1/V_a$  for each object in the survey so that the final LF reflects the incompleteness correction.

Although we attempt to correct for incompleteness in our survey, there are certain classes of hosts we may miss in a systematic fashion due to limitations in galaxy modeling and our selection technique for detecting compact nuclei. Such classes could include faint dwarf ellipticals with steep profiles. However, we note that for galaxies near  $L^*$  the sample should be reliably determined by total magnitude.

## 6.2. Comparison with the Local Luminosity Function for Seyferts

Figure 12 is the luminosity function for nuclei having colors consistent with Seyferts. Here we have plotted  $\log(\phi)$  in units of  $\# \text{ Mpc}^{-3} \text{ mag}^{-1}$  vs. the absolute B magnitude. The apparent V magnitudes were used to determine B magnitudes using equation 4. Table 1 provides the data used to construct this figure, including the number of data points in each bin  $n$  and the number corrected for incompleteness  $n_{\text{corrected}}$ . The luminosity function shown is for point sources contributing  $\geq 3\%$  of the total galaxy light. Figure 12 is the luminosity function with  $H_o=100 \text{ km s}^{-1} \text{ Mpc}^{-1}$ ,  $q_o=0.5$  and  $\alpha=-1.0$ . The thin solid line represents the LF at  $0 < z \leq 0.4$  and the dashed line represents the LF at  $0.4 < z \leq 0.8$ . The mean redshift of the low z bin is  $\langle z \rangle = 0.31$  and for the high z bin is  $\langle z \rangle = 0.57$ . We compare our LF with that of HB for Seyfert 1 and 2 galaxies from the CfA redshift survey (thick solid line).

Our LFs appear to be in good agreement with that of HB and maintain the same shape within the overlapping magnitude region,  $-18.5 \geq M_B \geq -20.5$ . Recent X-ray observations support the HB number density. The *Einstein* Extended Medium Sensitivity Survey (EMSS) provides an X-ray selected sample of LLAGN for which the optical luminosity function has been derived (Della Ceca et al. 1996). They used 226 broad-line AGN from this survey with measured redshifts and V magnitudes. Their LF extends to the same limiting absolute magnitude as that of HB and they find good agreement with their number density for broad-line AGNs. Here we have compared the present data with the HB LF for both Seyfert 1 and 2 type galaxies. Although the EMSS result is only for Seyfert 1 galaxies, it confirms the number density of broad line LLAGNs locally through a different selection method supporting the HB number density at faint absolute magnitudes.

To provide a more careful check on the possibility of increase or decrease between our LFs and that of HB within their overlapping luminosity range, we consider the number density of nuclei in our sample which are similar to the Seyfert nuclei of HB. Granato et al.

(1993) have shown that Seyfert nuclei from the CfA survey and other Markarian Seyferts have nuclei which contribute 20% to 100% of the total galaxy light. If we limit our LF to include only our nuclei that comprise more than 20% of the galaxy light, and are therefore more like those objects included in the HB study, we find the number density to decrease by a factor of 1.25 from that shown in Figure 12 for the LF at  $M_B = -19$  and  $-20$ . This amount of decrease is still consistent with our number density being the same as that of HB in these luminosity bins. We can further attempt to improve the comparison by correcting for possible incompleteness in the HB data due to the observed axis ratio bias of their sample illustrated in Maiolino & Rieke (1995). Accordingly, the HB data may be incomplete by a factor of 2. Correcting their LF for this level of incompleteness and comparing with our corrected LF, the number densities at  $M_B = -19$  and  $-20$  remain the same within the errors and are consistent with no change in the number density of LLAGN over this luminosity range. A statistical test is done by computing the density weighted  $1/V_a'$  number density (discussed in the following paragraph) for our nuclei in the overlapping luminosity bins and determining if the amount of density increase is statistically significant when compared to the HB number density in the same luminosity range. This test reveals that the two datasets are consistent with no density evolution within the errors.

Focusing now on the faint end of our LFs we notice that our upper limit luminosity functions for LLAGNs appear to flatten in both the high and low redshift bins at  $M_B \geq -16$ . The implication of this observed flattening with regard to quasar evolution models is discussed in detail later in this chapter. There does not appear to be evidence for a significant increase in number density between our high redshift LF and the low redshift LF within the Poisson errors. However, the high redshift LF consistently lies above the low redshift LF. This is most obvious at  $M_B \geq -18$ . To determine if the density increase is statistically significant, we use the  $\langle V'/V_a' \rangle$  method where  $V_a'$  is the density weighted accessible volume (Schmidt & Green 1983). Since our LFs are nearly parallel, we assume

luminosity independent density evolution of the form  $\rho(z)=(1+z)^\beta$ . The mean value of  $V'/V_a'$  is

$$\langle V'/V_a' \rangle = 0.5 \pm (12n)^{-1/2} \quad (7)$$

for objects distributed according to the assumed density equation. We begin our test by assuming no density evolution ( $\beta=0$ ) which yields  $\langle V'/V_a' \rangle = 0.602$ . We then increase  $\beta$  until  $\langle V'/V_a' \rangle = 0.5 \pm 0.043$ . The value of  $\langle V'/V_a' \rangle$  falls within this range ( $\leq 0.543$ ) at  $\beta=1.9$ , which represents the least amount of statistically significant density evolution to describe our data at  $z \leq 0.8$ .

Because our data represent upper limits of the AGN LF, this apparent increase in number density at the faint end should be carefully interpreted. If our selection technique systematically includes more objects at high redshift than at low redshift, the increase may not be real. However, we have shown that the nuclear region unresolved by HST increases slowly with redshift, varying only by 250 parsecs in diameter over the range  $0.2 \lesssim z \lesssim 0.8$ . One would need a significant population of nuclear objects having actual sizes between 300 and 550 pc in diameter so that they would appear unresolved in the higher redshift bin but appear resolved and therefore not included in the low redshift bin.

A test can be performed to determine if the increased number density observed for our unresolved nuclei could be due to a population of nuclear objects which appear unresolved at high  $z$  while remaining resolved at low  $z$ . Based on the distribution of bulge sizes in our study, we simply count the number of bulges that would appear unresolved if the number density of bulges in our survey remained constant down to bulge diameters of zero. In this way, we assume an upper limit number density for the small bulge population. We compare the number of bulges which would be observed in the lower redshift half of the survey as compared to the upper redshift half where we divide equally the volume of space. Equal volumes of space are measured at  $0 \leq z \leq 0.447$  and  $0.447 \leq z \leq 0.8$ . In this experiment, we

find that the number of unresolved bulges would remain constant within the Poisson errors between the two redshift bins of equal volume. We find that the number of nuclear point sources in our survey increases by a factor of 1.65 between the low redshift and the high redshift bins which is a statistically significant number density increase within the Poisson errors. This simple test indicates that the observed increase in number density could not be due to unresolved bulge-like objects in our survey.

Another test of the number density increase is conducted by performing the  $\langle V'/V_a' \rangle$  calculation over a smaller range in redshift. By limiting the redshift range, we reduce any effect on the observed number density evolution caused by marginally resolved nuclear objects becoming unresolved and adding to the number density at higher  $z$ . If we limit ourselves to performing this calculation for objects observed out to  $z=0.4$ , we find that the least amount of density evolution necessary to describe the observations is consistent with that required to describe the data out to  $z=0.8$ .

For the reasons we have outlined here, we interpret the increase in number density as resulting from an actual increase in the population of LLAGNS and nuclear starburst regions at  $-18 \leq M_B \leq -14$ . This observation poses the following question: if we observe an increase in number density at the faint end of our LF ( $M_B \leq -18$ ) but no increase at  $M_B = -19$  to  $-20$  as compared with HB, what are the implications for the global evolution of active nuclei? One explanation is that the population mix at the faint end is different from that at the bright end. Where we overlap with the LF of HB, our nuclei are likely to be more like the traditional Seyfert 1 galaxies. This is supported by the spectroscopic identifications of our two brightest nuclei. However, as we look at less luminous nuclei, we are probing a mix of fainter Seyfert 2s and LINERS. This population reveals an increase in number density with redshift out to  $z \simeq 0.8$  whereas the brighter Seyfert 1 nuclei do not show any number density evolution out to this redshift. In the following section, we discuss further the

implications of this scenario for comparing our observations with the intrinsically brighter QSO LFs.

### 6.3. Comparison with QSO Luminosity Functions

Figure 13 is the luminosity function with  $H_o=50$  km s $^{-1}$  Mpc $^{-1}$ ,  $q_o=0.5$  and  $\alpha=-0.5$ . Again, the solid line represents the LF from  $0 < z \leq 0.4$  and the dashed line is for  $0.4 < z \leq 0.8$ . Here we compare with the LF for QSO’s from the compilation by Hartwick and Schade (1990) for QSO’s having  $0.16 < z \leq 0.4$  (solid line at higher luminosities) and  $0.4 < z \leq 0.7$  (dashed line at higher luminosities). These redshift bins are roughly comparable to ours. Table 2 provides the data used to construct these LFs.

This figure is useful for studying how the LF at fainter absolute magnitudes compares with the bright end and allows us to investigate the nature of the luminosity function evolution. There is some indication in this figure that the shape of the LF changes between the low and high redshift bins when we consider both the low (this study) and high (Hartwick & Schade) luminosity points. If we assume that our upper limit LFs represent LLAGNs which are of the same nature as the brighter QSOs, any change in the overall shape of the LF would argue against both pure density evolution and pure luminosity evolution for these objects. Pure density evolution of the quasar LF has been ruled out by results from a large number of quasar surveys (e.g. Cheney & Rowan-Robinson 1981). In pure density evolution, the past LF is the same in shape as the local LF but shifted to higher densities. An overview of quasar evolution models can be found in Koo (1986). In pure luminosity evolution, a uniform shift to brighter luminosities is observed while the LF shape is preserved. Under these assumptions, the combined LFs in Figure 13 do not appear to favor either of these scenarios although we examine this question further below.

There have been many analytical representations for the shape of the quasar LF proposed in the literature. The double power-law model of Boyle et al. (1988) is well-constrained and adequately describes the data at  $z \lesssim 2.2$ . This model can be written as

$$\phi(L, z) = \frac{\phi_*/L_z}{(L/L_z)^{\beta_l} + (L/L_z)^{\beta_h}} \quad (8)$$

where the redshift dependence,  $L_z$ , is

$$L_z = L_*(1+z)^{-(1+\alpha)} \exp[-(z-z_*)^2/2\sigma_*^2] \quad (9)$$

as in Pei (1995) where pure-luminosity evolution is assumed and  $\alpha$  is the spectral index. In equation 8  $\beta_l$  is the power-law index for the faint end while  $\beta_h$  represents the bright end. To better compare our LF with the brighter quasar LF from Hartwick & Schade, we extrapolate this model, fitted to their data, to lower luminosities.

Figure 14a shows the LFs from Figure 13 with the double power-law model fit to the high luminosity data shown as the dotted line. The fitted parameters from Pei (1995) are  $\beta_l=1.64\pm0.18$ ,  $\beta_h=3.52\pm0.11$ ,  $z_*=2.75\pm0.05$ ,  $\sigma_*=0.93\pm0.03$ ,  $\log(L_*/L_\odot)=13.03\pm0.10$ , and  $\log(\phi_*/\text{Mpc}^3)=-6.05\pm0.15$ . These parameters are the best fit to the Hartwick & Schade LFs at various redshift bins. Here we have calculated the model at the median redshift for each of the two redshift bins to overlay with the LFs. Although the fit to the high luminosity LFs is very good, this model does not fit our LFs at lower luminosities. The model predicts lower number counts than our observations in the low redshift bin at  $-19 \leq M_B \leq -16$  and in the high redshift bin at  $-19 \leq M_B \leq -17$ . We also note that the model predicts lower number counts than that observed by HB as inferred from the agreement in Figure 12 between their LF and our data over the common absolute magnitude range.

Because our luminosity function is only an upper limit on the AGN LF at moderate redshifts, it is not necessarily in disagreement with the extrapolated number counts of the model fits. As described previously, even if we assume that the nuclei in our survey are

non-thermal in nature, our LF is likely to include an increased population of low-luminosity AGNs such as LINERS and faint Seyfert 2 nuclei. The extrapolated results of this model using the fitted parameters described above may be consistent with the population of faint QSOs and Seyfert 1 galaxies but may underestimate the total number of AGN including Seyfert 2s and LINERS at  $M_B \geq -22$ .

In Figure 14b we show the same LFs with the double power-law model fitted to both sets of data using  $\chi^2$  minimization. The fitted parameters are  $\beta_l=1.6$ ,  $\beta_h=3.4$ ,  $\log(L_*/L_\odot)=12.5$  and  $\log(\phi_*/\text{Mpc}^3)=-5.2$  holding  $z_*$  and  $\sigma$  constant at the fitted values of Pei. The flattening of the LF in the faint data is not well fit by this model. The  $\chi^2$  of the fit to this combined data set indicates a worse fit than that obtained for the bright quasar data alone in several redshift bins. We notice that the largest change in the fitted parameters occurs in the normalization and inflection point of the double power-law model and not in the slopes. Our two brightest LF bins, which are consistent with the HB local LF, largely influence the fit in this manner. If the two data sets being combined here are actually representing the same type of active nucleus, this result indicates that the double power-law model assuming pure luminosity evolution is not the best representation of the data. The transition region between the low and high luminosity data appears to require a model with additional variables for adequate fitting of this portion of the LF.

This result leads to the following question: without considering the bright quasar data from Harwick & Schade, how well does pure luminosity evolution (PLE) model our faint LF over the redshift range to  $z=0.8$ ? We fit a simple power-law to our low and high redshift LFs and determine the amount of PLE necessary to adequately model the data.

A power-law is fit to both the high and low redshift LFs from  $-18 \leq M_B \leq -14$  of the form

$$\log\phi(z) = \text{const} + \gamma M(z) \quad (10)$$

where  $\gamma$  is the slope of the  $\log\phi$ - $M$  relation and is found to be  $0.079 \pm 0.066$ . We find the

mean increase in  $\log\phi$  over this magnitude range is 0.4. This  $\Delta\log\phi$  divided by  $\gamma$  gives the change in magnitude,  $\Delta M=5.1^{+25.7}_{-2.3}$ . For pure luminosity evolution

$$\Delta M = 2.5\delta\log((1+z_{high})/(1+z_{low})) \quad (11)$$

Here,  $\delta$  is the amount of PLE necessary to account for the observed density increase in a power-law parameterization in  $(1+z)$ . Using the mean  $z$  for each of our LF bins, we determine  $\delta=25.8^{+130.1}_{-11.6}$ . This simple calculation shows that the amount of PLE necessary to account for the observed density increase is unreasonably large and unlikely to explain the observations.

The fact that our LF is only an upper limit probably does little to remedy the flatness of the faint end of the AGN LF. Any population of objects which may be included in our survey, such as intermediate aged starburst nuclei or minor merger remnants, is likely to have a luminosity function with a negative slope at the faint end similar to that observed in the normal galaxy LF. If this is the case, subtracting an LF of this shape from our upper limit would result in further flattening of the faint end of the AGN LF.

## 7. The Number of LLAGN in Local Spiral Galaxies

In this section we address the implications the observed number density of compact nuclei in our survey has for the lifetimes of LLAGN and the fraction of present-day spiral galaxies that may host AGN of low luminosities. We first make the assumption that the observed number density increase with redshift is caused by the evolution of LLAGNs. As we will describe further in the following section, we assume a Gaussian density evolution equation for these objects consistent with the observed mild density evolution to  $z=0.8$  but turning over at  $z=2.3$  (see equation 16). At their peak density at  $z=2.3$ , the total number of unresolved nuclei is  $5.9\times10^{-3}$   $\text{Mpc}^{-3}$   $\text{mag}^{-1}$  with  $H_0=100$   $\text{km s}^{-1} \text{Mpc}^{-1}$ . If our

sample consists entirely of LLAGNs, what fraction of present-day galaxies are likely to have contained an LLAGN at some point in their lives? Typically our nuclei are found in spiral galaxies with absolute magnitudes in the range  $-20.5 \leq M_B \leq -18.5$ . Using the LF of Marzke et al. (1994) for spiral galaxies, the number of local spirals in this absolute magnitude range is  $9 \times 10^{-3}$  per Mpc<sup>3</sup>. This result implies that almost all present-day spiral galaxies contain LLAGN with absolute magnitudes of  $M_B \simeq -16$  at some epoch, some of which may now be dormant. The total number density at  $z=1.0$ , which requires less extrapolation of our observations, indicates that  $\sim 40\%$  of present-day spiral galaxies contain LLAGN in this magnitude range. If we assume the observed luminosity of these objects is due to disk accretion onto a black hole, we can determine if the amount of matter necessary to fuel an AGN of this luminosity over a Hubble time is plausible. We convert the absolute magnitude to bolometric luminosity based on  $L_{bol}/L_B = 11.8 \pm 4.3$  for quasars from Elvis et al. (1994). An order of magnitude approximation for the implied  $\dot{M}$  is given by

$$\dot{M} \sim L_{bol} (10^{-9} M_{\odot}/yr) / (10^{37} ergs/s) \quad (12)$$

from Shapiro & Teukolsky (1983). For nuclei with  $M_B = -16$ ,  $\dot{M}$  equals  $8 \times 10^{-4} M_{\odot}/yr$ . After 15 Gyr, the object accretes  $\sim 10^7 M_{\odot}$ , comparable to the mass of the black hole, which is a reasonable amount of matter for accretion. This result has interesting implications on the search for AGN in local galaxy nuclei.

## 8. Implications For the X-Ray Source Surface Density

Quasars have long been known as strong X-ray emitters and statistically significant samples have been selected through X-ray surveys (e.g. Giacconi et al. 1979). How quasars and their low-luminosity counterparts contribute to the diffuse X-ray background has been a question of interest for some time. In particular, low-luminosity AGNs are considered good candidates for explaining the origin of the soft X-ray background (0.2 - 4.0 keV).

Schmidt and Green (1986) derived the contribution of LLAGNs ( $M_B > -23$ ) to be 29% of the observed background at 2 keV assuming no evolution in the number density. They note that any substantial evolution would dramatically increase this value. Other studies indicate that 30% to 90% of the background at 2 keV originates from AGNs (Boyle et al 1993) but with the brightest AGN making up 30%. Could the rest of the soft background be comprised of LLAGN?

We calculate the likely contribution of the compact nuclei in our survey to the X-ray background based on assumptions about the X-ray nature of the nuclei. Let us assume that the X-ray flux of our nuclei is most like that for fainter AGN such as Seyfert 2s and LINERS. From the *Einstein Observatory* Imaging Proportional Counter (IPC), soft X-ray spectra for 22 Seyfert 2s and some LINERS in the range of 0.2 to 4.0 keV have been obtained (Kruper et al. 1990) and the X-ray luminosity for these objects is  $10^{42 \pm 0.72}$  erg s<sup>-1</sup>. In order for these galaxies to be spectroscopically classified as Seyfert 2s or LINERS, the nucleus must contribute a large fraction of the total galaxy light. From the CfA redshift survey, we know that spectroscopically selected Seyferts have nuclei contributing between 20% and  $\sim 100\%$  of the total galaxy light (Granato et al. 1993). Because our nuclei are roughly an order of magnitude fainter, we assume their X-ray flux is also an order of magnitude fainter and is likely to be closer to  $1 \times 10^{41 \pm 0.72}$  erg s<sup>-1</sup>. This rough estimate is in good agreement with the soft X-ray flux of 5 LLAGNs measured with ROSAT *HRI* (Koratkar et al. 1995). They range in x-ray luminosity from  $10^{40.2}$  to  $10^{41.4}$  erg s<sup>-1</sup>.

We first assume that the LFs we observe consist entirely of LLAGN and that there is mild number density evolution of these objects over the absolute magnitude range  $-18 \lesssim M_B \lesssim -14$ . Since the LF is relatively parallel over this magnitude range in both redshift bins, we allow the number density to be independent of luminosity for these objects where

$$\log \phi = 1.9 \log(z + 1) - 4.09 \quad (13)$$

for  $H_o=50 \text{ km s}^{-1} \text{ Mpc}^{-1}$ ,  $q_o=0.5$  and  $\alpha=-0.5$  and where  $\phi$  is in units of  $\text{Mpc}^{-3} \text{ mag}^{-1}$ .

To determine the total X-ray flux for these objects, we integrate the number density  $\phi(z)$  multiplied by the X-ray flux out to  $z_{max}$ .

$$I_{Tot} = \int_0^{Z_{max}} \phi(z) \frac{L_x}{4\pi A^2(z)} \frac{dV}{dz} dz \quad (14)$$

where  $I_{Tot}$  is the total X-ray flux from the point source nuclei. The volume element is defined in Avni (1978) as

$$dV/dz = \omega(c/H_o) A^2(z) (1+z)^{-3} (1+2q_o z)^{-0.5} \quad (15)$$

We assume a Gaussian form for the number density evolution consistent with the mild evolution observed out to  $z=0.8$  (equation 13) but reaching a maximum near  $z=2.3$ , the apparent peak in the quasar number density from Schmidt, Schneider & Gunn (1991). This is written as

$$\phi(z) = 1.03 \times 10^{-3} (1+z)^{-0.5} \exp(-(z-2.3)^2/2) \quad (16)$$

in units of  $\text{Mpc}^{-3} \text{ mag}^{-1}$ . The integration out to  $z_{max}=4.0$  over 4 magnitude bins ( $-18 \leq M_B \leq -14$ ) yields a total X-ray flux of  $10^{-8.84 \pm 0.72} \text{ ergs s}^{-1} \text{ cm}^{-2} \text{ sr}^{-1}$  for the 0.2 - 4.0 keV range.

A recent measurement of the X-ray background using ROSAT (Chen, Fabian & Gendreau 1997) found an intensity of  $1.46 \times 10^{-8} \text{ ergs s}^{-1} \text{ cm}^{-2} \text{ sr}^{-1}$  in the 1 - 2 keV range. Hasinger et al. (1993) find an X-ray background intensity of  $1.25 \times 10^{-8} \text{ ergs s}^{-1} \text{ cm}^{-2} \text{ sr}^{-1}$  for this energy range. To convert between the measured energy ranges for comparison, we assume a power-law X-ray spectral index of  $\alpha_x=-0.5$  based on *Einstein Observatory* IPC observations of low luminosity AGNs consisting primarily of Seyfert 2s and LINERS (Kruper et al. 1990). The conversion factor from the 0.2 - 4.0 keV to the 1 - 2 keV range is 0.267. Assuming an X-ray background intensity of  $1.36 \times 10^{-8}$  for 1 - 2 keV (an average of the two measured values), our nuclei between  $-18 \leq M_B \leq -14$  contribute up to 15% of the X-ray

background. If we assume a steeper spectral index of  $\alpha_x = -1.5$ , as suggested by Koratkar et al. (1995) for LLAGNs, our nuclei contribute up to 10% of the X-ray background.

Because we do not have actual X-ray flux measurements for the galaxies in our sample, these estimates of their contribution to the soft X-ray background are based on assumptions about the X-ray nature of these objects. Although we cannot say with certainty what their true contribution is, these results suggest that LLAGN may contribute a relatively significant portion of the soft X-ray background but would not be able to make up the bulk of X-ray emission at these energy levels. Further study of the X-ray properties of faint AGN would provide tighter constraints on their likely contribution to the diffuse X-ray background.

## 9. Conclusions

This study explores the space density and properties of active galaxies to  $z \approx 0.8$ . We have investigated the frequency and nature of unresolved nuclei in galaxies at moderate redshift as indicators of nuclear activity such as AGN or starbursts. The main results and conclusions are as follows:

- Compact nuclei appear to favor host galaxies with bulges contributing less than 50% of the galaxy light. The majority of hosts have small bulges consistent with late-type spiral galaxies. The distribution of host galaxies more closely resembles that for nearby starbursting galaxies than local dwarf Seyfert nuclei but could be consistent with some combination of these two populations.
- The host galaxies of compact nuclei have smaller half-light radii as compared to the entire sample of survey galaxies. Very few of the large, faint galaxies in the survey contain compact nuclei. This may be a result of low surface brightness galaxies being stable against

the growth of bar instabilities which may help fuel nuclear activity. The host galaxy colors are generally like those of other morphologically similar galaxies in the field with a slight tendency to be bluer. We also note that compact nuclei avoid host galaxies with low disk axis ratios ( $(b/a) \lesssim 0.4$ ) although to a much lesser degree than spectroscopically selected samples of Seyferts. This slight effect may be caused by obscuration in a flattened disk parallel to the plane of the host galaxy or by the main disk containing dust extending into the galaxy center.

- The distribution of absolute magnitudes for the host galaxies peaks at  $M_B \simeq -21.3$  with  $H_o = 50 \text{ km/s/Mpc}$  which is very similar to that for local Seyfert hosts. This distribution is consistent with that for local LLAGN and HII nuclei hosts found by Ho et al. (1997a and 1997b).
- Most of the nuclei have colors consistent with Seyfert nuclei and also consistent with intermediate age star clusters. A small number have colors too blue to be Seyferts but are consistent with young or intermediate aged star clusters and are likely to be starburst nuclei.
- Using the subsample of nuclei having colors consistent with Seyfert and intermediate age starburst nuclei, we construct the upper limit luminosity function for faint AGN out to redshifts of  $z \simeq 0.8$  providing the first look at the shape and parameters of the AGN LF in this luminosity and redshift regime. Our upper limit LF compares well with that for Seyferts in the CfA redshift survey (Huchra & Burg 1992) with no evidence for an increase in the number density over their common magnitude range. However, a mild increase in the number density of compact nuclei is detected between our low ( $\langle z \rangle = 0.31$ ) and high ( $\langle z \rangle = 0.57$ ) redshift LFs of the form  $\phi \propto (1+z)^{1.9}$  for nuclei at  $-18 \lesssim M_B \lesssim -14$  ( $H_o = 50 \text{ km/s/Mpc}$ ). The mild number density evolution at the faint end of our LFs could be the result of an increase in the fraction of Seyfert 2 nuclei and LINERS in this luminosity range.

- Both the low and high redshift LFs for our data appear to flatten at  $M_B \geq -16$ . When compared with the bright quasar LFs from Harwick & Schade (1990), the overall shape of the LF appears to change from low to high redshift arguing against pure density and pure luminosity evolution if our LFs represent the intrinisically fainter counterparts of QSOs. However, this apparent change in shape may be caused in part by the possibility that our fainter LFs contain a greater fraction of Seyfert 2 nuclei and LINERS. The flatness of our LF at these faint magnitudes and the increase in number density is inconsistent with pure luminosity evolution within our observations. Additionally, we find the number density of our nuclei combined with the observed mild evolution indicates that almost all present-day spiral galaxies could host LLAGN either active or dormant.
- Assuming the X-ray flux of our nuclei to be similar to that of Seyfert 2s and LINERs, we estimate these nuclei in the range  $-18 \leq M_B \leq -14$  can contribute up to 10 – 15% of the soft X-ray background at 1 to 2 keV. Further study of the X-ray properties of faint AGN is needed to provide tighter constraints on their likely contribution to the diffuse X-ray background.

## 10. Future Work

The results of this study provide the first look at the population of LLAGNs at moderate redshifts. Many additional questions can be studied with this dataset to understand better the processes that create and maintain nuclear activity in galaxies. In the cases of both AGN and starbursts, mechanisms are required within the host galaxy to provide fuel for the nuclear activity. Many such mechanisms have been proposed such as bars, galaxy-galaxy interactions, and other morphological disturbances. These types of disturbances have been well studied in local groups of galaxies giving only the current picture of how host galaxy morphology relates to nuclear activity. Studying a population

of active galaxies at earlier epochs will help us understand how such fueling mechanisms evolve on a global scale over several gigayears.

For example, determining the frequency of bars in AGN/starburst hosts to  $z \approx 0.8$  would allow us to trace the global evolution of bars in initiating nuclear activity. If a higher frequency of bars is detected at high  $z$  while decreasing towards lower  $z$ , the typical duration of a bar in an active galaxy as well as the likely formation epoch can be estimated. This scenario is consistent with the lack of a bar/AGN connection observed locally (McLeod & Rieke 1995; Ho et al. 1997c). If the bar frequency remains constant with  $z$ , bars might be forming at a rate close to the rate at which they dissolve. Another globally interesting question can be answered by studying the control sample of field galaxies. Since many galaxies may have experienced episodes of rapid star formation, tracing the evolution of bars and other asymmetries in the control sample will help us understand when and how these perturbations have affected the general population of galaxies. We can also determine how the presence of a bar affects the AGN/starburst luminosity.

In order to more directly compare the results of this survey to spectroscopic surveys, the morphologies of these survey galaxies must be examined in the same way as our HST imaged galaxies. Such a study will bring to light the differences and biases in these survey techniques. High resolution ground-based images for a sample of local low-luminosity Seyfert galaxies would allow us to study the nuclear regions and determine the fraction in which the AGN can be morphologically detected. Likewise, HST images are available for many fields where spectroscopic follow-up has been obtained with the CFHT and Keck telescopes. Spectroscopic selection of active galaxies in these surveys can then be compared with the morphological evidence of an active nucleus. The results of such studies will allow for a more direct comparison of the number density of local AGNs to more distant ones observed with HST.

We would like to thank the referee and editor for comments and suggestions which have improved the quality of this paper. The authors would like to thank John Huchra and Rogier Windhorst for helpful discussions and guidance on this project. We are also grateful to Caryl Gronwall for providing software and models to estimate galaxy K-corrections. In addition, we thank Yichen Pei for providing us with QSO luminosity function models and model fitting software. This work is based on observations taken with the NASA/ESA *Hubble Space Telescope*, obtained at the Space Telescope Science Institute, operated by the Association of Universities for Research in Astronomy, Inc. This work was supported in part by STScI grant GO-02684.06-87A to R. F. G. for the Medium Deep Survey project.

## REFERENCES

Avni, Y. 1978 *A&A*, 63, L13

Bade, N., Fink, H. H., Engels, D., Voges, W., Hagen, H.-J., Wisotzki, L. & Reimers, D. 1995, *A&AS*, 110, 469

Balzano, V. A. 1983, *ApJ*, 268, 602

Boroson, T. 1981, *ApJS*, 46, 177

Boyle, B. J., Griffiths, R. E., Shanks, T., Stewart, G. C. & Georgantopoulos, I. 1993, *MNRAS*, 260, 49

Boyle, B. J., Shanks, T. & Peterson, B. A. 1988, *MNRAS*, 235, 935

Bruzual, A. G. & Charlot, S. 1993, *ApJ*, 405, 5

Chen, L.-W., Fabian, A. C. & Gendreau, K. C. 1997, *MNRAS*, 285, 449

Cheng, F. Z., Danese, L., De Zotti, G. & Franchesini, A. 1985, *MNRAS*, 212, 857

Cheney, J. E. & Rowan-Robinson, M. 1981, *MNRAS*, 195, 497

Christensen, C. G. 1975, *AJ*, 80, 282

Della Ceca, R., Zamorani, G., Maccacaro, T., Setti, G. & Wolter, A. 1996, *ApJ*, 465, 650

Elvis, M., Soltan A. & Keel, W. C. 1984, *ApJ* 283, 479

Elvis, M., Wilkes, B. J., McDowell, J. C., Green, R. F., Bechtold, J., Willner, S. P., Oey, M. S., Polomski, E. & Cutri, R. 1994, *ApJS*, 95, 1.

Friedli, D. & Benz, W. 1993, *A&A*, 268, 65

Giacconi, R. et al. 1979, *ApJ*, 234, L1

Granato, G. L., Zitelli, V., Bonoli, F., Danese, L., Bonoli, C. & Delpino, F. 1993, *ApJS*, 89,

Griffiths, R. E. et al. 1994, *ApJ* 437, 67

Gronwall, C. & Koo, D. C. 1995, *ApJ*, 440, L1

Hassinger, G., Burg, R., Giacconi, R., Hartner, G., Schmidt, M., Trumper, J. & Zamorani, G. 1993, *A&A*, 275, 1

Hartwick, F. D. A. & Schade, D. 1990, *ARA&A*, 28, 437

Hibbard, J. E., Guhathakurta, P., van Gorkom, J. H. & Schweizer, F. 1994, *AJ*, 107, 67

Ho, L. C., Filippenko, A. & Sargent, W. L. W. 1997a, *ApJS*, 112, 315

Ho, L. C., Filippenko, A. & Sargent, W. L. W. 1997b, *ApJ*, 487, 579

Ho, L. C., Filippenko, A. & Sargent, W. L. W. 1997c, *ApJ*, 487, 591

Huchra, J. & Burg, R. 1992, *ApJ*, 393, 90

Keel, W. C. 1980, *AJ*, 85, 198

Kennicutt, R. C. 1992, *ApJS*, 79, 255

Koo, D. C. 1986, in *Structure and Evolution of Galactic Nuclei*, eds. G. Guiricin et al., p. 317

Koo, D. C. et al. 1996, *ApJ*, 469, 535

Koratkar, A., Deustua, S. E., Heckman, T., Filippenko, A. V., Ho, L. C. & Rao, M. 1995, *ApJ* 440, 132

Kotilainen, J. K. & Ward, M. J. 1994, *MNRAS*, 266, 953

Kruper, J. S., Urry, C. M. & Canizares, C. R. 1990, *ApJS*, 74, 347

Lawrence, A. & Elvis, M. 1982, *ApJ*, 256, 410

Leitherer, C. et al. 1996, *PASP*, 108, 996

Nelson, C. H., MacKenty, J. W., Simkin, S. M. & Griffiths, R. E. 1996, *ApJ*, 466, 713

McLeod, K. K. & Rieke, G. H. 1995, *ApJ*, 441, 96

Maiolino, R. & Rieke, G. H. 1995, *ApJ*, 454, 95

Malkan, M. A., Gorjian, V. & Tam, R. 1998, *ApJS*, 117, 25

Mihos, J. C., McGaugh, S. S. & de Blok, W. J. G. 1997 *ApJ*, 477, L79

Pei, Y. C. 1995, *ApJ*, 438, 623

Sarajedini, V. L., Green, R. F., Griffiths, R. E. & Ratnatunga, K. U. 1998, submitted  
(Paper I)

Schweizer, F. 1996, *AJ*, 111, 109

Schmidt, M. & Green, R. F. 1983, *ApJ*, 269, 352

Schmidt, M. & Green, R. F. 1986, *ApJ*, 305, 68

Schmidt, M., Schneider D. P. & Gunn, J. E. 1991, in "The Space Distribution of Quasars",  
Proceedings of the Workshop, Victoria, Canada, ed. D. Crampton, p. 109

Shapiro, S. L. & Teukolsky, S. A. 1983, in "Black Holes, White Dwarfs, and Neutron Stars:  
The Physics of Compact Objects", John Wiley & Sons, Inc.

Tresse, L., Rola, C., Hammer, F., Stasinska, G., Le Fevre, O., Lilly, S. J. & Crampton, D.  
1996, *MNRAS*, 281, 847

Weedman, D. W., Feldman, F. R., Balzano, V. A., Ramsey, L. W., Sramek, R. A. & Wuu,  
C.-C. 1981, *ApJ*, 248, 105

Williams, R. E. 1996, *AJ*, 112, 1335

Yee, H. K. 1983, *ApJ*, 272, 473

## FIGURE CAPTIONS

Fig. 1.— a) The fraction of galaxies in the Monte-Carlo simulation where the measured Bulge/Total is zero as a function of the input Bulge/Total for the galaxy. The errorbars are the Poisson statistics based on the number of galaxies in each bin. b) The distribution of Bulge/Bulge+Disk measurements for galaxies containing compact nuclei. The solid line is the actual number distribution. The two dashed lines represent two extremes of the distribution after statistically correcting for bulge misclassification as described in the text.

Fig. 2.— Histogram of measured Bulge/Total values for the 1033 galaxies in our survey (hatched region) normalized by 1:500. The dotted line represents the total fraction of galaxies in each Bulge/Total bin.

Fig. 3.— a) The galaxy I magnitude vs. the natural log of the half-light radius of the galaxy for all survey galaxies (open circles) and those galaxies containing compact nuclei (filled circles). b) The normalized distribution of half-light radii for all survey galaxies (solid line) and those containing compact nuclei (hatched region).

Fig. 4.— Histogram of the axis ratios for galaxies containing compact nuclei. The histogram is normalized by dividing by the axis ratio histogram for all spiral survey galaxies.

Fig. 5.— a) The color-magnitude diagram for galaxies in our survey where open circles represent non-host galaxies and filled circles represent those galaxies hosting a compact nucleus. b) The normalized histogram of galaxy V-I colors for the host galaxies (hatched region) compared with the normalized histogram of galaxy colors for a representative group of non-host galaxies of similar morphological type (solid line).

Fig. 6.— a) Histogram of rest-frame B absolute magnitudes for the host galaxies in our sample. b) Absolute B magnitudes from Ho et al. (1997a) of dwarf Seyfert nuclei hosts. c)

Absolute B magnitudes from Ho et al. (1997b) of HII nuclei hosts.

Fig. 7.— a) The point source V-I color vs. the host galaxies V-I color. Points measured in only one filter are shown as color limits. b) The generalized histogram of the color difference between the host galaxy and the point source.

Fig. 8.— a) The point source V-I color vs. the bulge V-I color for the 17 galaxies containing a measureable bulge and point source color. b) The generalized histogram of the color difference between the bulge and the point source nucleus.

Fig. 9.— The redshift vs. the V-I color of the unresolved nuclei. The open circles represent color limits for some nuclei.

Fig. 10.— a) Seyfert 1 spectrum produced by averaging several reliably classified Seyfert 1 galaxies (Kalinkov et al. 1993). b) Seyfert 1.5 galaxy spectrum. c) Seyfert 2 galaxy spectrum. d) HII nucleus from E. Bica in Leitherer et al. (1996). e) age $\simeq$ 10 Myr star cluster with  $[Z/Z_{\odot}] \simeq -0.25$ . f) age $\simeq$ 25 Myr star cluster with  $[Z/Z_{\odot}] \simeq -0.4$ . g) age $\simeq$ 80 Myr star cluster with  $[Z/Z_{\odot}] \simeq -0.5$ . h) age $\simeq$ 200-500 Myr star cluster with  $[Z/Z_{\odot}] \simeq -0.6$ . i) age $\simeq$ 1-2 Gyr star cluster with  $[Z/Z_{\odot}] \simeq -0.5$ . The y-axes are in flux density units of  $\text{ergs s}^{-1} \text{ cm}^{-2} \text{ \AA}^{-1}$  normalized at 5600 $\text{\AA}$  to 10.

Fig. 11.— a) V-I colors for the 3 types of Seyfert galaxies as a function of redshift. The solid line is the Seyfert 2 color, the short dashed line is the Seyfert 1.5 and the long dashed line is the Seyfert 1. b) V-I colors for various star cluster spectra as a function of redshift. The solid line is the integrated HII region color, the short dashed line is the 10 Myr cluster, the long dashed line is the 25 Myr cluster, the dot-short dashed line is the 80 Myr cluster, the dot-long dashed line is the 200-500 Myr cluster, and the dotted line is the 1-2 Gyr cluster.

Fig. 12.— The luminosity function of compact nuclei  $\geq 3\%$  of the total galaxy light. The

thin solid line represents the LF for nuclei at  $0 < z \leq 0.4$  and the dashed line is the LF at  $0.4 < z \leq 0.8$ . The thick solid line is the LF for Seyfert galaxies from the CfA redshift survey (Huchra & Burg 1992). Here we have assumed  $H_o = 100 \text{ km s}^{-1} \text{ Mpc}^{-1}$ ,  $q_o = 0.5$  and  $\alpha = -1.0$ .

Fig. 13.— The luminosity function of compact nuclei  $\geq 3\%$  of the total galaxy light. The solid line represents nuclei at  $0 < z \leq 0.4$  and the dashed line is for  $0.4 < z \leq 0.8$ . At higher luminosities we show the LF for QSO's from the compilation by Hartwick and Schade (1990) for  $0.16 < z \leq 0.4$  (solid line at  $M_B \leq -22$ ) and  $0.4 < z \leq 0.7$  (dashed line at  $M_B \leq -22$ ). Here we have assumed  $H_o = 50 \text{ km s}^{-1} \text{ Mpc}^{-1}$ ,  $q_o = 0.5$  and  $\alpha = -0.5$ .

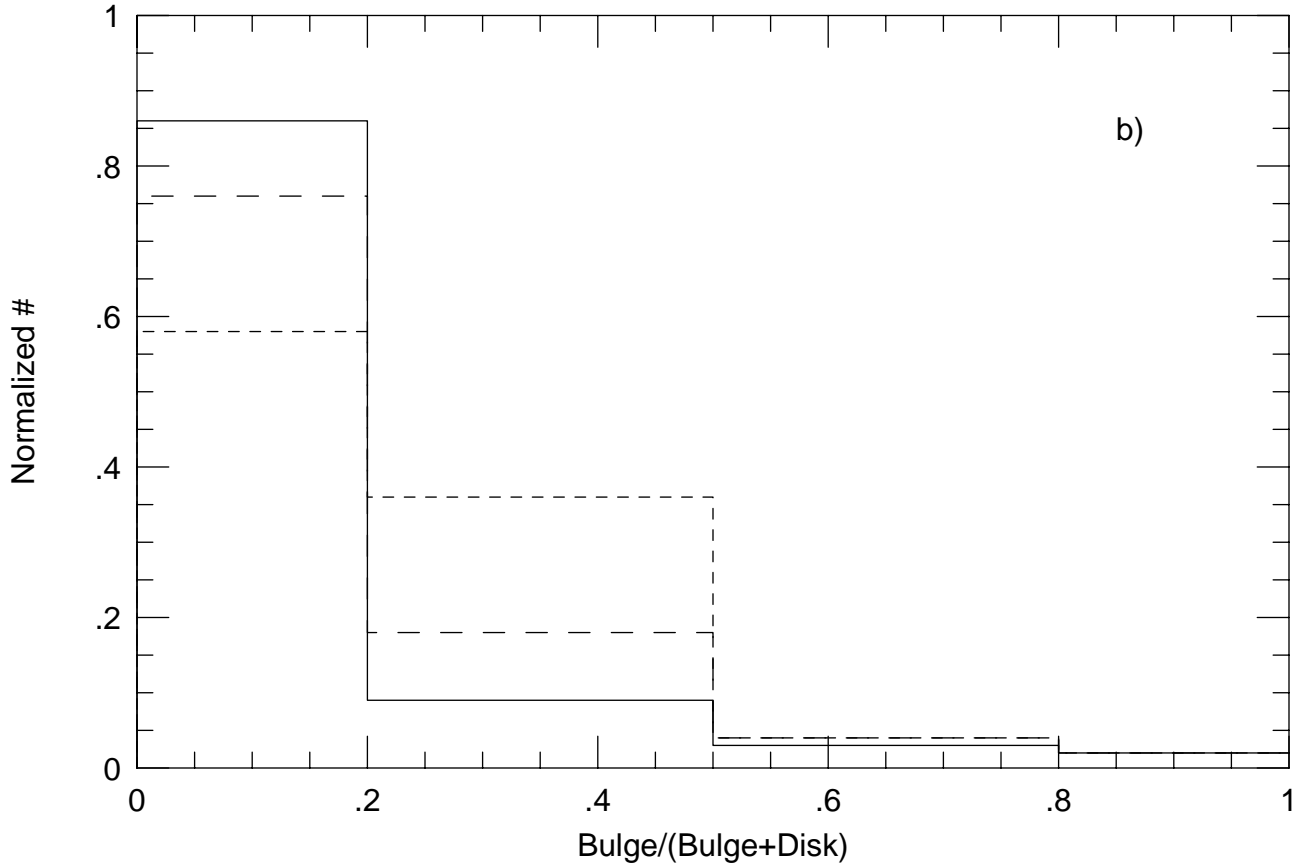
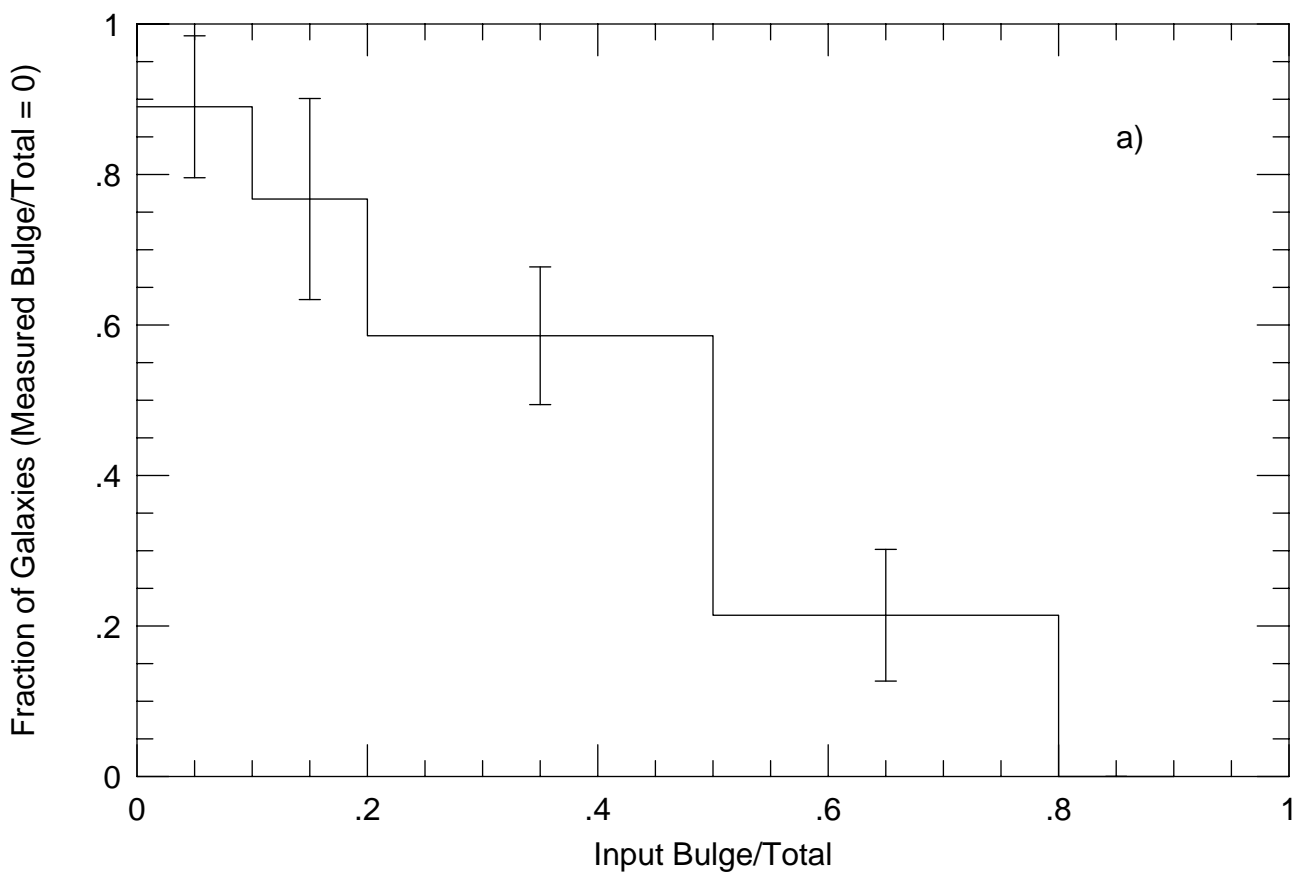
Fig. 14.— a) The double power-law model fitted to the bright quasar LFs (dotted line) using parameters from Pei (1995). b) The same model fitted to both the bright LF and the faint LF (this data). We assume  $H_o = 50 \text{ km s}^{-1} \text{ Mpc}^{-1}$ ,  $q_o = 0.5$  and  $\alpha = -0.5$ .

Table 1. Luminosity Functions ( $H_o=100$ ,  $q_o=0.5$  and  $\alpha=-1.0$ )

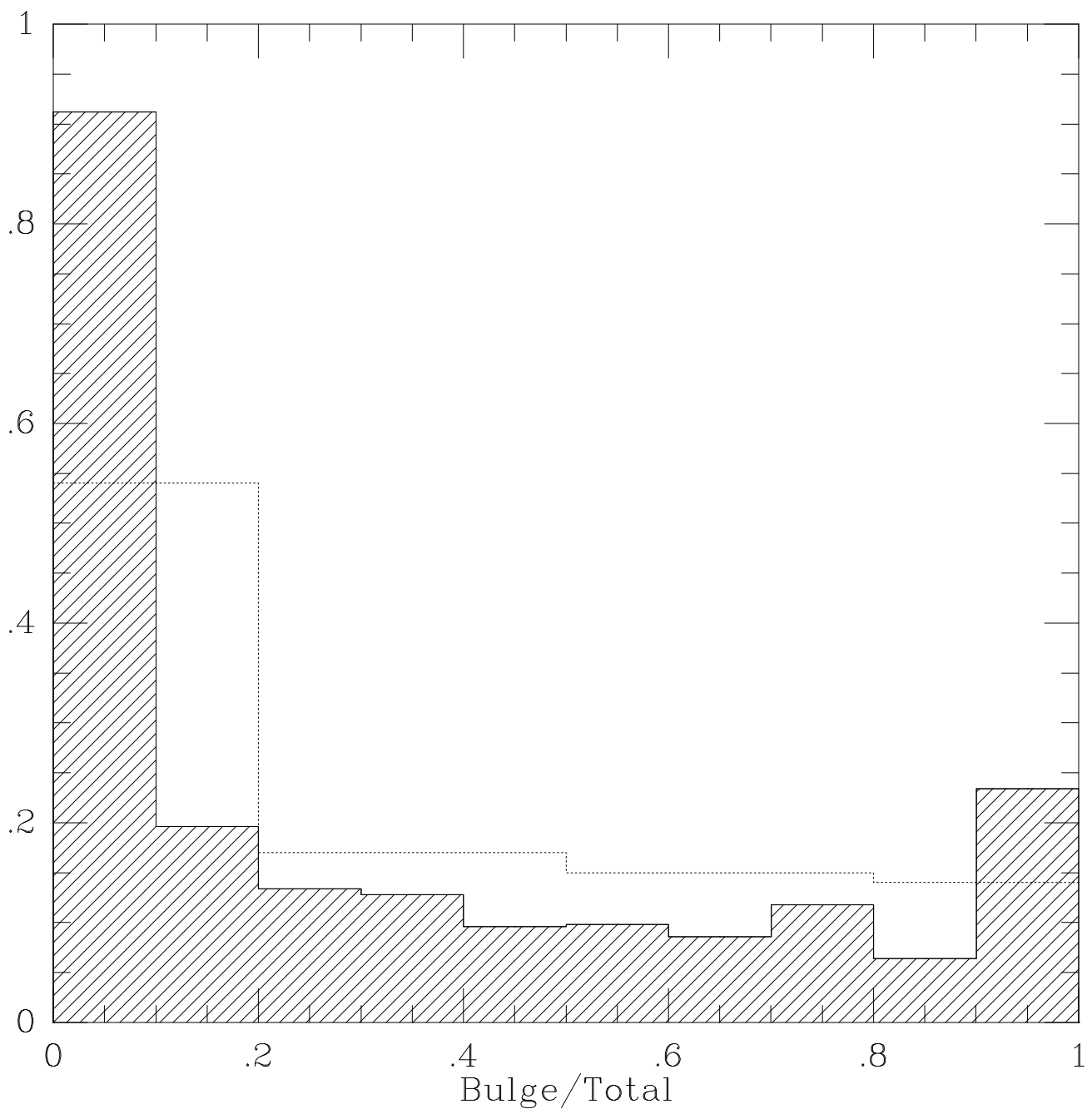
$M_B$	$\phi$	n	$n_{corrected}$	$\phi$	n	$n_{corrected}$	
$0 < z \leq 0.4$				$0.4 < z \leq 0.8$			
-13.0	-3.02	0.33	1.20	-2.64	0.08	0.31	
-14.0	-2.65	2.26	6.13	-2.26	0.63	2.44	
-15.0	-2.81	3.01	9.92	-2.61	2.58	7.51	
-16.0	-2.94	3.17	9.10	-2.58	8.79	21.43	
-17.0	-3.09	2.96	6.55	-2.94	7.63	17.22	
-18.0	-3.64	0.99	1.90	-3.35	3.50	5.46	
-19.0				-4.18	1.02	1.54	
-20.0				-4.21	1.06	1.61	

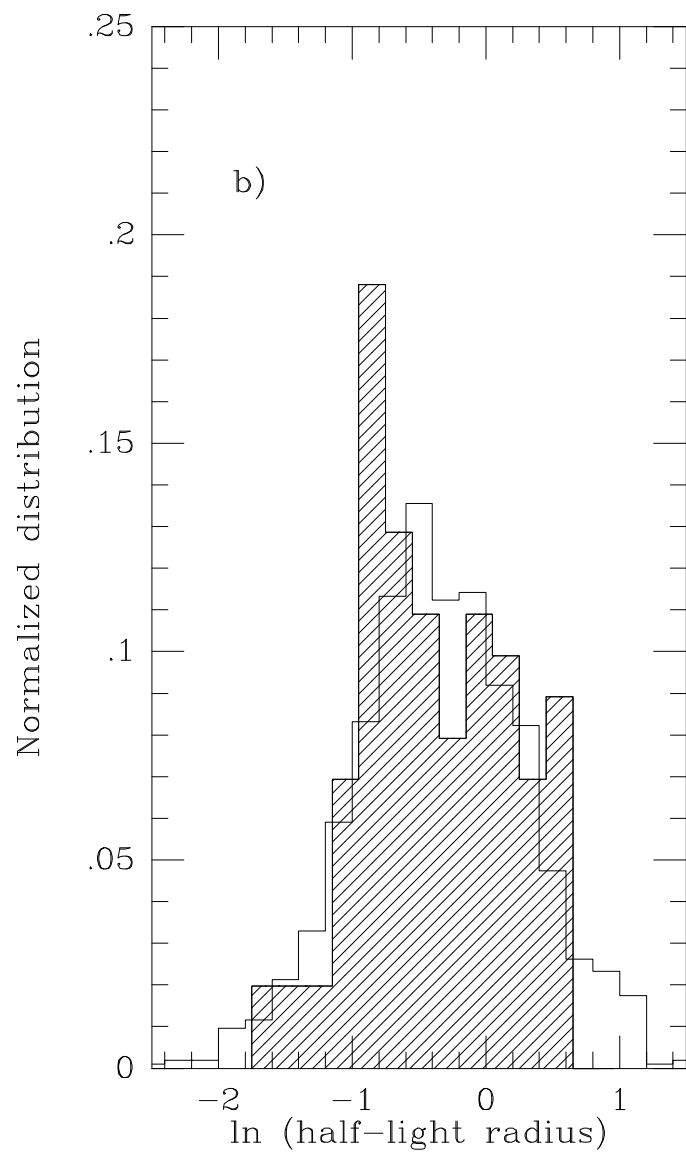
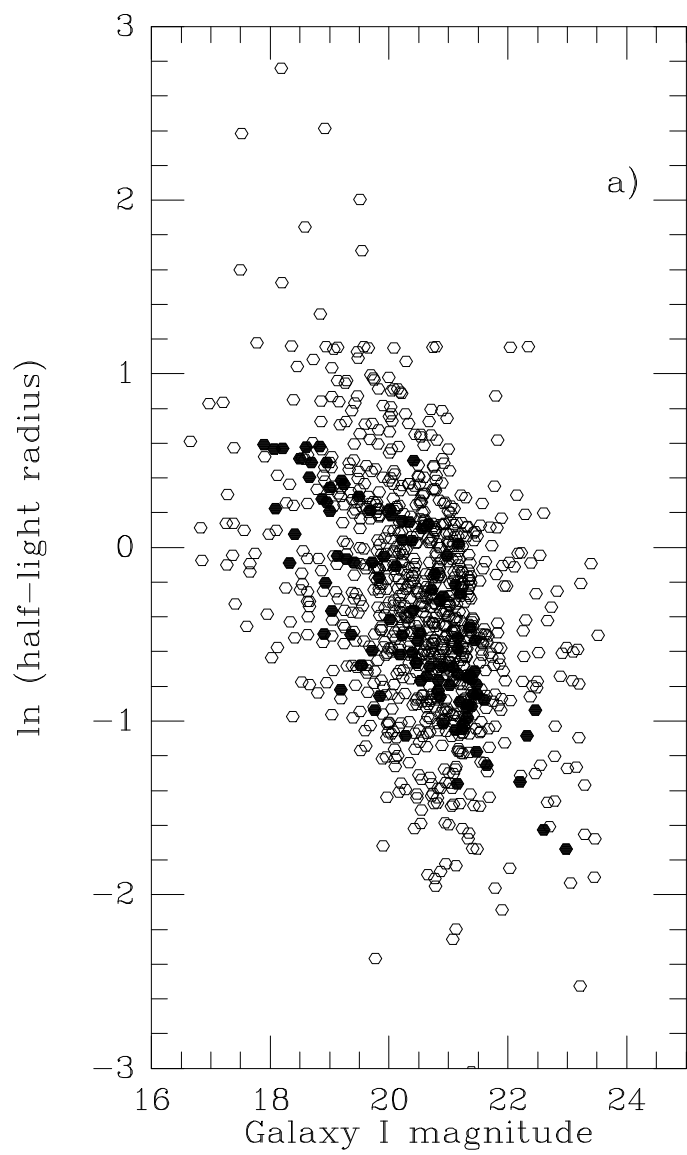
Table 2. Luminosity Functions ( $H_o=50$ ,  $q_o=0.5$  and  $\alpha=-0.5$ )

$M_B$	$\phi$	n	$n_{corrected}$	$\phi$	n	$n_{corrected}$	
$0 < z \leq 0.4$				$0.4 < z \leq 0.8$			
-13.0	-3.81	0.06	0.21				
-14.0	-3.98	0.16	0.58				
-15.0	-3.87	0.64	2.27	-3.10	0.50	1.94	
-16.0	-3.51	3.23	9.40	-3.64	1.03	3.68	
-17.0	-3.73	3.47	11.12	-3.38	7.55	19.76	
-18.0	-3.99	2.33	6.65	-3.73	7.93	18.87	
-19.0	-4.11	2.97	5.02	-4.07	5.24	8.69	
-20.0				-4.75	1.68	2.55	
-21.0				-5.02	1.34	2.04	

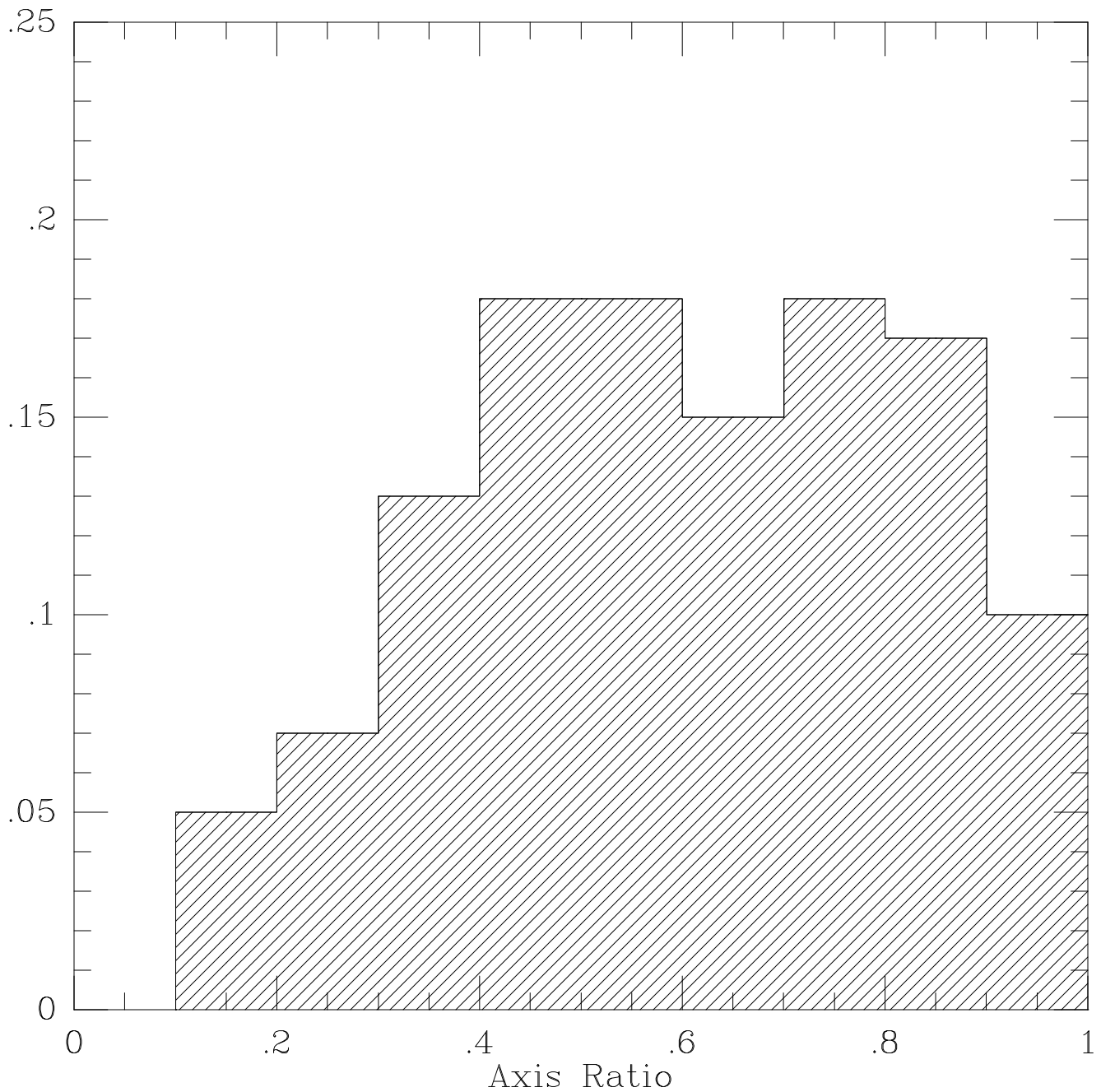


Fraction of Galaxies

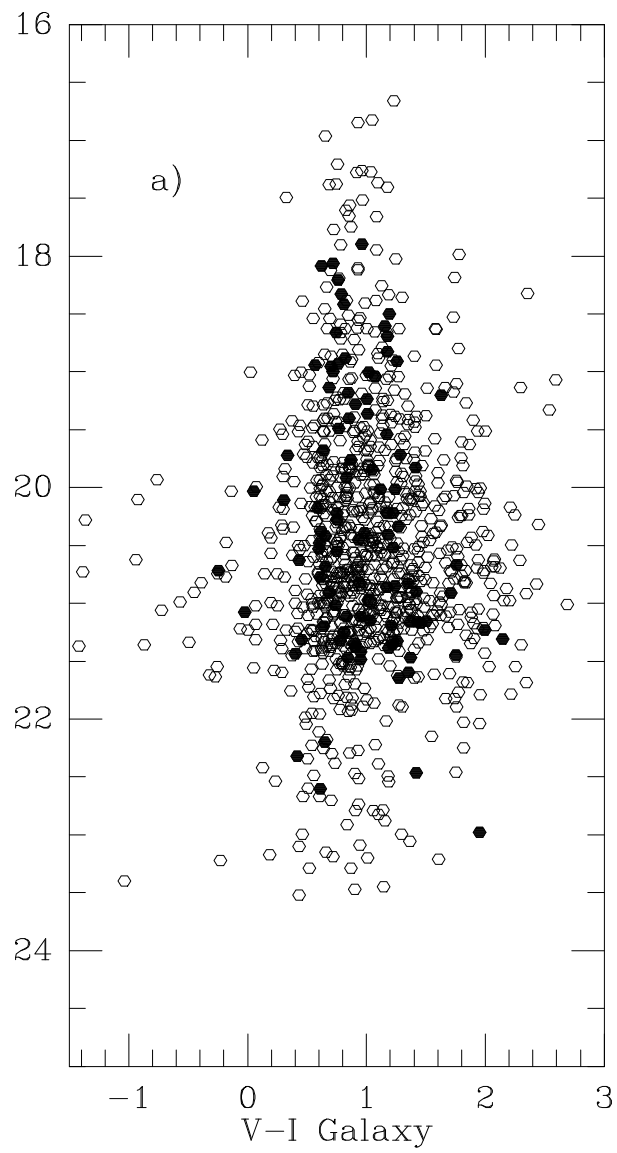




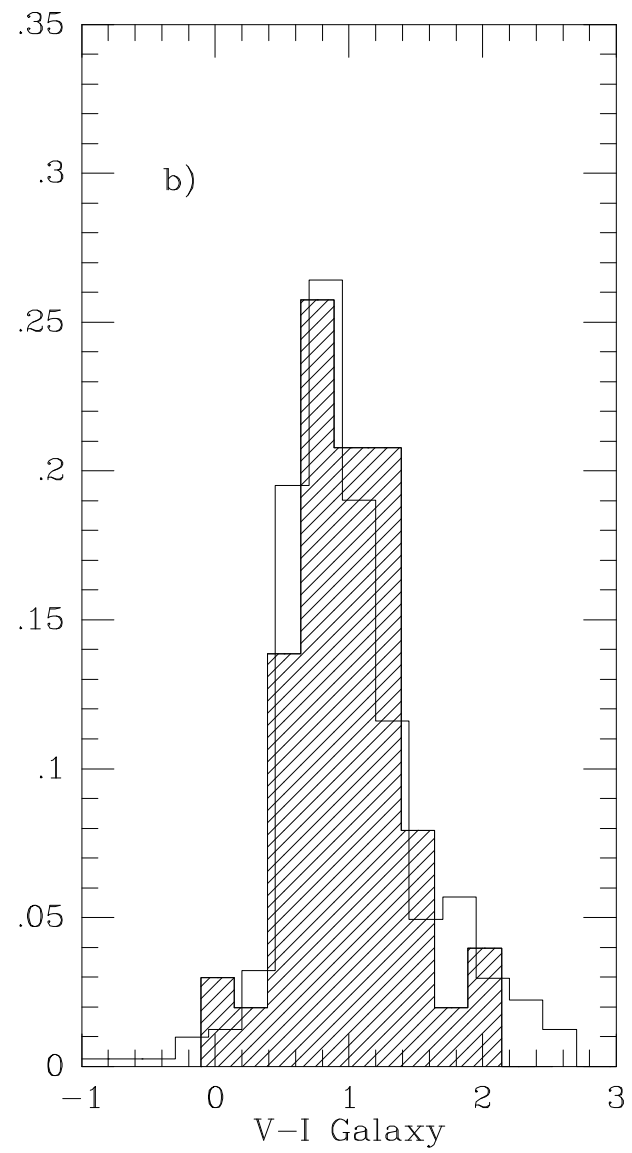
Fraction of Disk Galaxies Containing Compact Nuclei

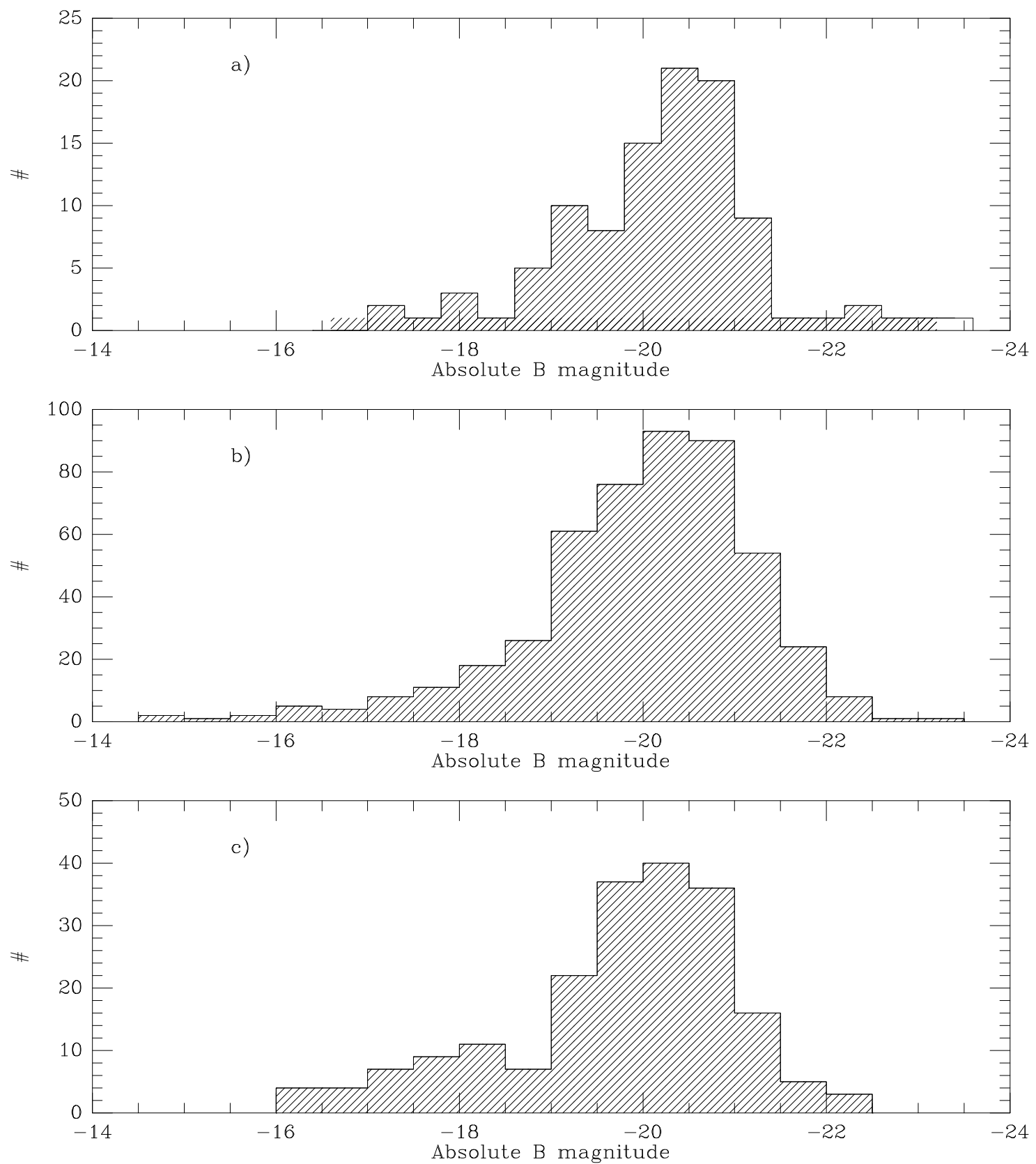


Integrated Galaxy I magnitude



Normalized #





Host galaxy V-I

